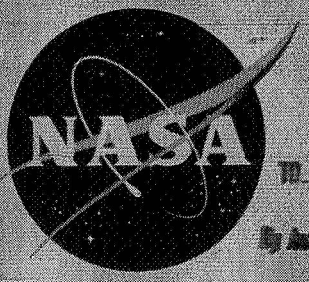

NASA TM X-558

TECHNICAL MEMORANDUM

X-558

LONGITUDINAL STABILITY AND CONTROL CHARACTERISTICS AT A MACH NUMBER OF 2.01 OF SEVERAL SIMULATED AIR-LAUNCHED BALLISTIC MISSILES HAVING VARIOUS TYPES OF CONTROL SURFACES

By Ross B. Robinson and M. Leroy Spearman

Langley Research Center
Langley Field, Va.

NATIONAL AERONAUTICS AND SPACE ADMINISTRATION
WASHINGTON
August 1961

NATIONAL AERONAUTICS AND SPACE ADMINISTRATION

TECHNICAL MEMORANDUM X-558

LONGITUDINAL STABILITY AND CONTROL CHARACTERISTICS AT A MACH NUMBER OF 2.01 OF SEVERAL SIMULATED AIR-LAUNCHED BALLISTIC MISSILES HAVING VARIOUS TYPES OF CONTROL SURFACES*

By Ross B. Robinson and M. Leroy Spearman

SUMMARY

An investigation has been conducted in the Langley 4- by 4-foot supersonic pressure tunnel at a Mach number of 2.01 to determine the longitudinal stability and control characteristics of several simulated air-launched ballistic missiles. Various controls including a canard surface, rearward tails, and a forebody flap were investigated on a body representative of a two-stage ballistic missile.

The results indicated that the canard control alone was slightly more efficient than the tail control alone. With the two controls deflected simultaneously, a general increase in trimmed normal force was obtained over that for the separate controls with essentially no change in lift-drag ratio. Deflection of a forebody flap provided a reasonably linear increment in pitching moment throughout the angle-of-attack range but also produced a rather large increase in axial force.

INTRODUCTION

In order to obtain information on the stability and control characteristics of configurations that offer promise as hypersonic missiles, an investigation of a family of missile models has been undertaken. The initial phase of the investigation is reported in reference 1 for a Mach number of 2.01 and in reference 2 for Mach numbers of 2.29 to 4.65. The characteristics at Mach numbers of 2.01, 4.65, and 6.8 of two configurations, one having low-aspect-ratio cruciform wings with trailing-edge

flap controls and one having a flared afterbody and all-movable cruciform controls, are presented in reference 3. The stability and control characteristics at a Mach number of 2.01 of a configuration employing the trailing-edge flap controls of reference 3 as horizontal tails and cruciform all-movable wing controls are given in reference 4.

As an outgrowth of the previous studies, the investigation has been extended to include the determination of the stability and control characteristics of a configuration simulating a two-stage air-launched ballistic missile. The air-launched ballistic missile presents a unique control problem in that a high degree of controllability is required shortly after launch in order to maneuver from a near-horizontal launch attitude into a ballistic climb path. The investigation of controls for this purpose included the use of canard control surfaces as well as tail-rearward controls. In addition, the use of a forebody flap attached to the conical skirt of the second stage was investigated. A flap of this type might serve the dual purpose of providing pitch control for the initial trajectory maneuver as well as serving as a drag flap for reentry control of the second stage. The various controls were investigated separately and in combination for an angle-of-attack range up to about 26° in the Langley 4- by 4-foot supersonic pressure tunnel at a Mach number of 2.01 and a Reynolds number of 2.44×10^6 per foot.

COEFFICIENTS AND SYMBOLS

The results are referred to the body axis system except the lift and drag coefficients which are referred to the stability axis system. The moment reference point is at a longitudinal station corresponding to 50 percent of the body length. The coefficients and symbols are defined as follows:

C_L lift coefficient, $\frac{\text{Lift}}{qA}$

C_N normal-force coefficient, $\frac{\text{Normal force}}{qA}$

C_D drag coefficient, $\frac{\text{Drag}}{qA}$

C_A axial-force coefficient, $\frac{\text{Axial force}}{qA}$

C_m pitching-moment coefficient, $\frac{\text{Pitching moment}}{qA\ d}$

q	free-stream dynamic pressure
A	maximum cross-sectional area of the body, 7.07 sq in.
d	maximum body diameter, 3.00 in.
M	free-stream Mach number
α	angle of attack, deg
$\delta_{c,h}$	horizontal canard surface deflection, deg
$\delta_{c,v}$	vertical canard surface deflection, deg
δ_f	body flap deflection, deg
δ_t	rearward tail deflection of all four surfaces, deg
$\delta_{t,h}$	horizontal rearward tail deflection, deg
$\delta_{t,v}$	vertical rearward tail deflection, deg
l	length of body
x	distance from nose to moment reference point
L/D	lift-drag ratio

Components:

B	body
W_L	wing (large)
W_S	wing (small)
T	tail surfaces (in vertical and horizontal position)
T_{45}	tail surfaces (in 45° planes)
C	canard surfaces (vertical and horizontal)
C_h	canard surfaces (horizontal only)
f	forebody flap

MODELS AND APPARATUS

Details of the model are shown in figure 1 and the geometric characteristics are presented in table I.

The model was composed of a body, cruciform wings, and cruciform canard and tail controls. (See fig. 1(a).) The canard and tail surfaces were inline and the wings indexed 45°. When the wings were removed, the tails could be indexed 45° with respect to the canards. Two sizes of wings and a nose simulating an ICBM nose cone were provided. (See figs. 1(b) and 1(c).) Details of the canard and tail control surfaces are shown in figure 1(d). A body flap which was flush with the body contour was located on the conical transition section joining the nose to the afterbody. (See fig. 1(c).) Deflection of the nose flap, horizontal canards, and all tail surfaces were manually adjustable. When the nose flap was deflected, both of the vertical canards were removed. Sketches of the various configurations investigated are shown in figure 2.

The model was mounted in the tunnel on a remote-controlled rotary sting and force measurements were made through the use of a six-component internal strain-gage balance.

TESTS, CORRECTIONS, AND ACCURACY

The test conditions are as follows:

Mach number	2.01
Stagnation temperature, °F	100
Stagnation pressure, lb/sq ft	1,440
Reynolds number, per foot	2.44×10^6

The stagnation dewpoint was maintained sufficiently low (-25° F or below) so that no condensation effects were encountered in the test section. Tests were made through an angle-of-attack range of about -1° to 26°. The angle of attack was corrected for the deflection of the balance and sting under load. The base pressure was measured, and the drag force was adjusted to a base pressure equal to free-stream static pressure.

The estimated accuracy of the individual measured quantities is as follows:

C_N	±0.0140
C_A	±0.0016
C_m	±0.0080
α, deg	±0.2
$\delta_{c,h}$, deg	±0.1
δ_f, deg	±0.1
δ_t, deg	±0.1
M	±0.015

PRESENTATION OF RESULTS

The results of the investigation are presented in the following figures:

	Figure
Aerodynamic characteristics in pitch of various combinations of components	3
Effects of nose shape, BW_LC	4
Effects of canard deflection:	
BW_LCT, $\delta_{t,h} = 0^\circ$	5(a)
BW_LCT, $\delta_{t,h} = -20^\circ$	5(b)
BC_hW_S	6
BC_hT_{45}	7
BC_h	8
Effects of horizontal-tail deflection:	
BW_LCT	9
BW_LT	10
BC_hT_{45}	11
BT_{45}	12
Effects of body-flap deflection:	
BW_LTf, $\delta_{t,h} = 0^\circ$	13(a)
BW_LTf, $\delta_{t,h} = -20^\circ$	13(b)
Effects of combined canard and body-flap deflections:	
BW_LC_hTf, $\delta_{t,h} = -20^\circ$	14
BW_LC_hf	15
$BC_hT_{45}f$	16

Figure

SUMMARY OF RESULTS

A limited comparison of an ICBM nose shape with a spherical nose shape (fig. 4) indicated little effect on the aerodynamic characteristics of one configuration (BW_LC). All other configurations were tested with the spherical nose shape only.

Use of the canard surface as a pitch control provides a variation of pitching moment with canard deflection that decreases with increasing control deflection and with increasing angle of attack. In addition, the axial-force increment due to canard deflection increases with increasing angle of attack. (See figs. 5 to 8.) A nonlinearity in pitching moment near an angle of attack of 8° (particularly noticeable in figs. 6 and 7) is apparently an interference effect of the canard-surface flow field on the rearward surfaces. Deflection of the canard surface does provide a small positive increment in normal force at low angles of attack but this increment decreases and becomes negative with increasing angle of attack as a result of the downwash induced on the wings, tail, and afterbody.

Deflection of the horizontal tail as a pitch control (figs. 9 to 12) provides a reasonably linear variation of pitching moment with tail deflection that remains essentially constant throughout the angle-of-attack range. The presence of the canard surface has no effect on the pitching effectiveness of the tail control (figs. 9 and 10) although the nonlinearity previously noted in the pitching-moment variation with α due to the canard is still apparent (figs. 9 and 11). Deflection of the tail causes a negative increment in normal force throughout the angle-of-attack range but the axial-force increment due to tail deflection decreases with increasing α. With the wings removed and the tails rotated to 45° planes (figs. 11 and 12), a substantial increase in control effectiveness is obtained since all four tail surfaces are deflected to produce pitching moment. However, for a given angle of attack, considerably less normal force is available with the wings off than with the wings on.

The use of a forward body flap as a pitch control provides a reasonably linear increment in pitching moment throughout the angle-of-attack

range, which is accompanied, however, by a rather large increase in axial force. (See fig. 13.) An inspection of the results with various combined-control deflections for several configurations (figs. 13(b), 14, 15, and 16) indicate that the control effectiveness for the combined deflections is generally additive.

The trimmed longitudinal characteristics as a function of moment-reference location for configuration BW_LCT (fig. 17) indicate that the canard control alone (fig. 17(a)) is slightly more efficient than the tail control alone (fig. 17(b)). However, when the two controls are deflected simultaneously, a general increase in normal-force coefficient C_N was obtained over that for the separate controls with essentially no change in lift-drag ratio L/D.

Langley Research Center,
National Aeronautics and Space Administration,
Langley Field, Va., May 31, 1961.

REFERENCES

1. Robinson, Ross B.: Wind-Tunnel Investigation at a Mach Number of 2.01 of the Aerodynamic Characteristics in Combined Angles of Attack and Sideslip of Several Hypersonic Missile Configurations With Various Canard Controls. NACA RM L58A21, 1958.

2. Turner, Kenneth L., and Appich, W. H., Jr.: Investigation of the Static Stability Characteristics of Five Hypersonic Missile Configurations at Mach Numbers From 2.29 to 4.65. NACA RM L58D04, 1958.

3. Spearman, M. Leroy, and Robinson, Ross B.: Longitudinal Stability and Control Characteristics at Mach Numbers of 2.01, 4.65, and 6.8 of Two Hypersonic Missile Configurations, One Having Low-Aspect-Ratio Cruciform Wings With Trailing-Edge Flaps and One Having a Flared Afterbody and All-Movable Controls. NASA TM X-46, 1959.

4. Robinson, Ross B., and Foster, Gerald V.: Static Longitudinal Stability and Control Characteristics at a Mach Number of 2.01 of a Hypersonic Missile Configuration Having All-Movable Wing and Tail Surfaces. NASA TM X-516, 1961.

TABLE I.- MODEL DIMENSIONS

Body:		
Length, in.		30.00
Maximum diameter, in.		3.00
Base area, sq in.		7.07
Center of moments location, percent length		50
	Small	Large
Wings:		
Span, in.	1.80	1.80
Root chord, in.	4.50	9.00
Tip chord, in.	2.70	7.20
Area, per pair, sq in.	12.96	29.16
Thickness, in.	0.188	0.188
Leading-edge sweep angle, deg	45	45
Canard surfaces:		
Area, per pair, sq in.		4.48
Thickness, in.		0.188
Leading-edge sweep angle, deg		45
Tail surfaces:		
Span, in.		1.34
Chord, in.		3.00
Area, per pair, sq in.		8.04
Thickness, in.		0.188
Leading-edge sweep angle, deg		0
Body flap:		
Area, projected, sq in.		6.13
Included angle, deg		135

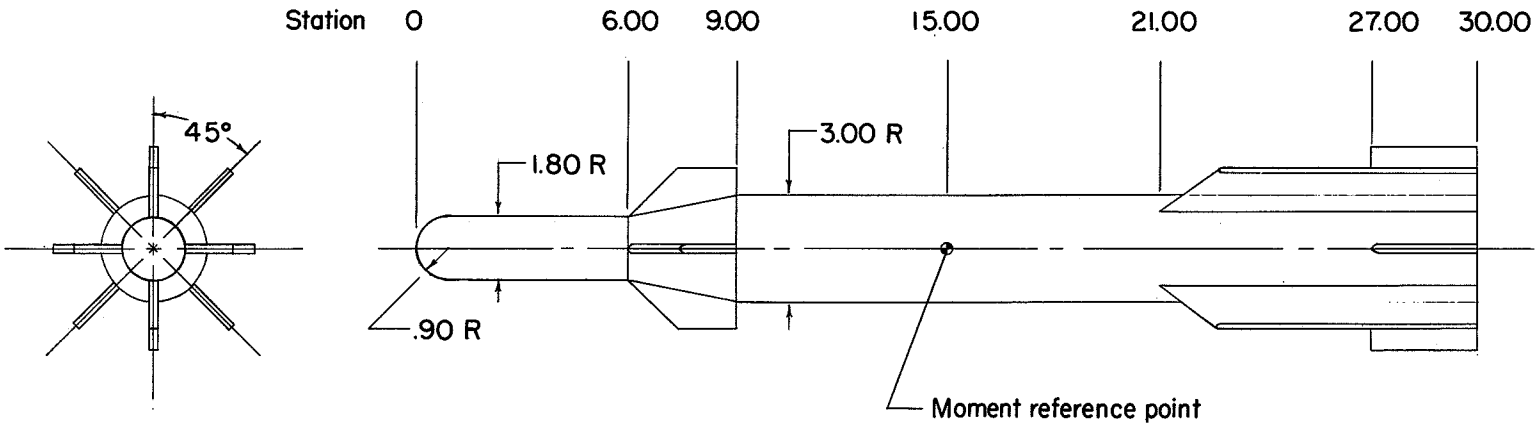

(a) General arrangement of complete model.

Figure 1.- Details of model.

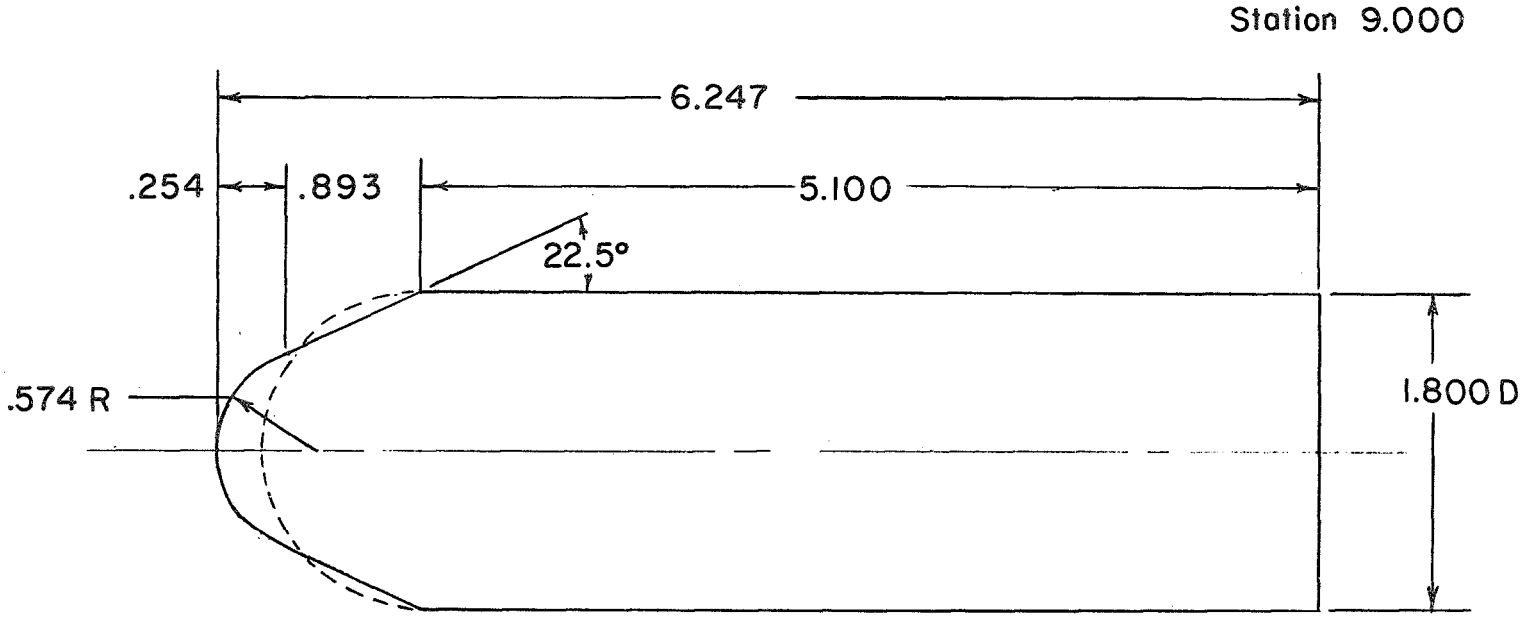

(b) Details of ICBM nose. Spherical nose shown as dashed line.

Figure 1.- Continued.

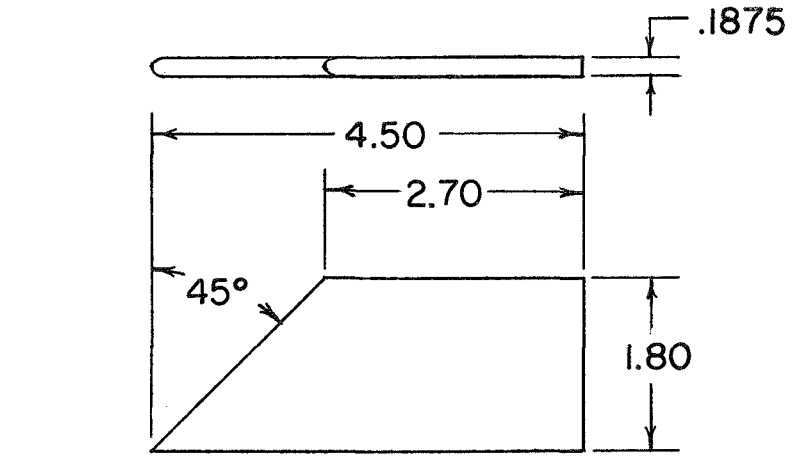

Small

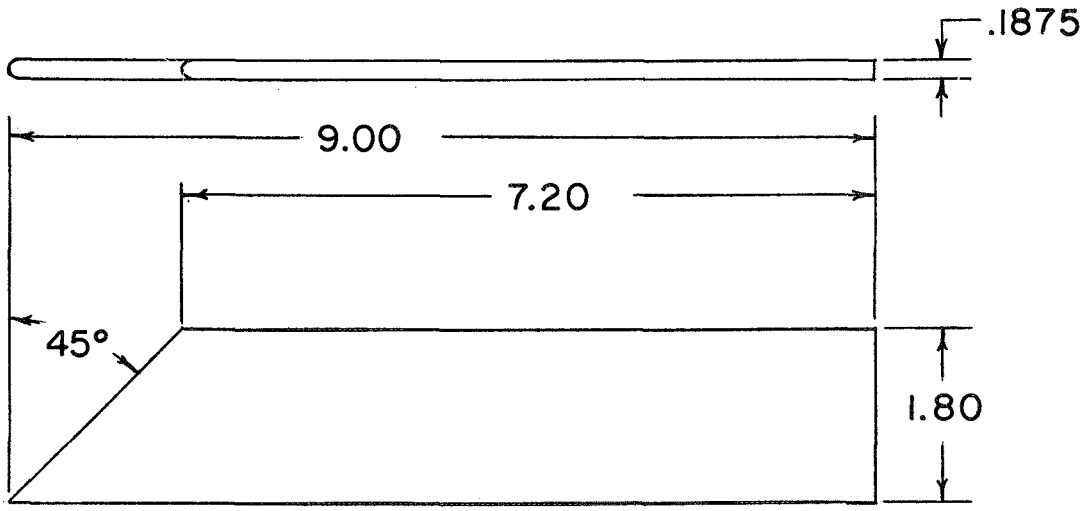

Large

(c) Details of wings.

Figure 1.- Continued.

(d) Control surfaces.

Figure 1.- Continued.

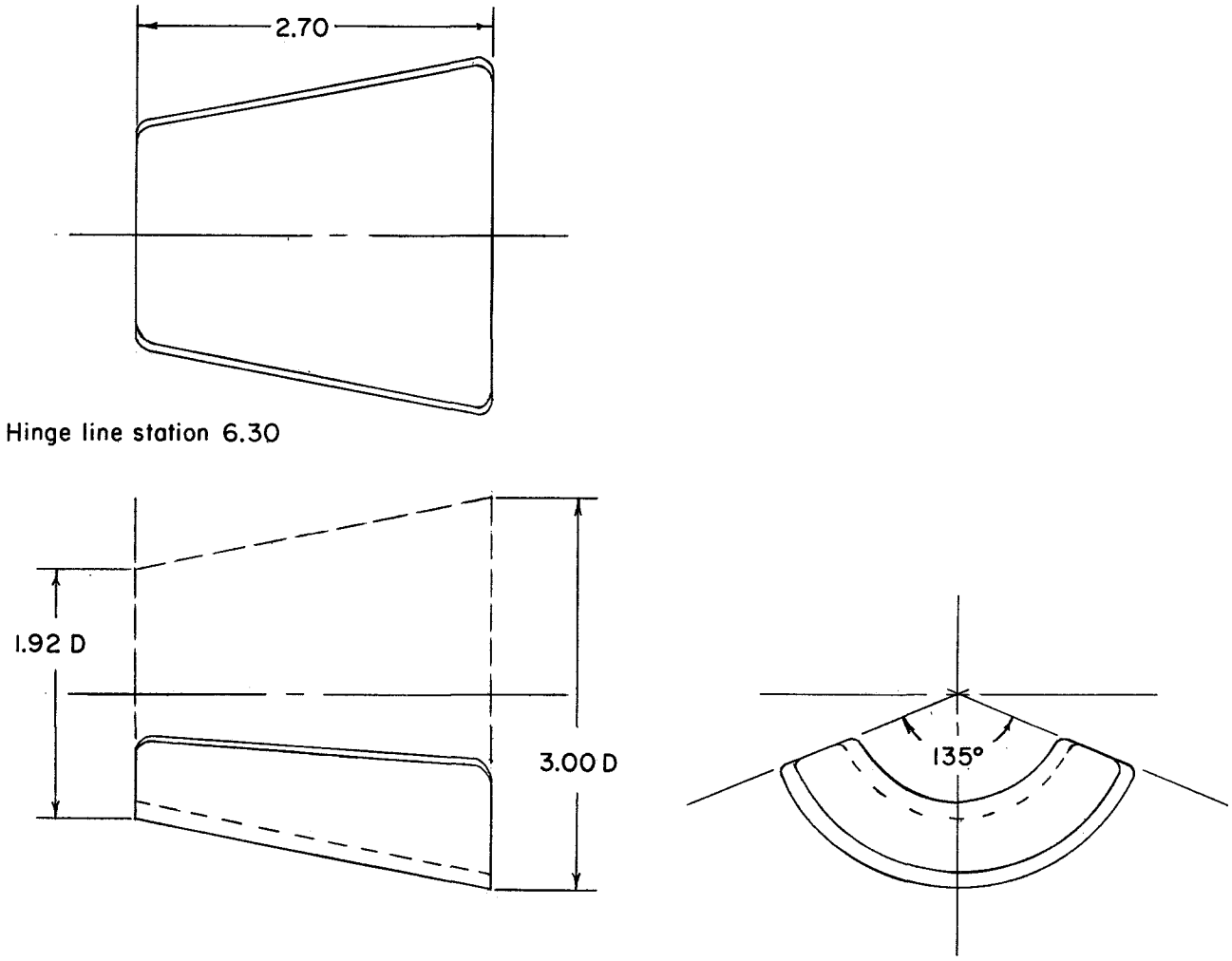

(e) Body flap.

Figure 1.- Concluded.

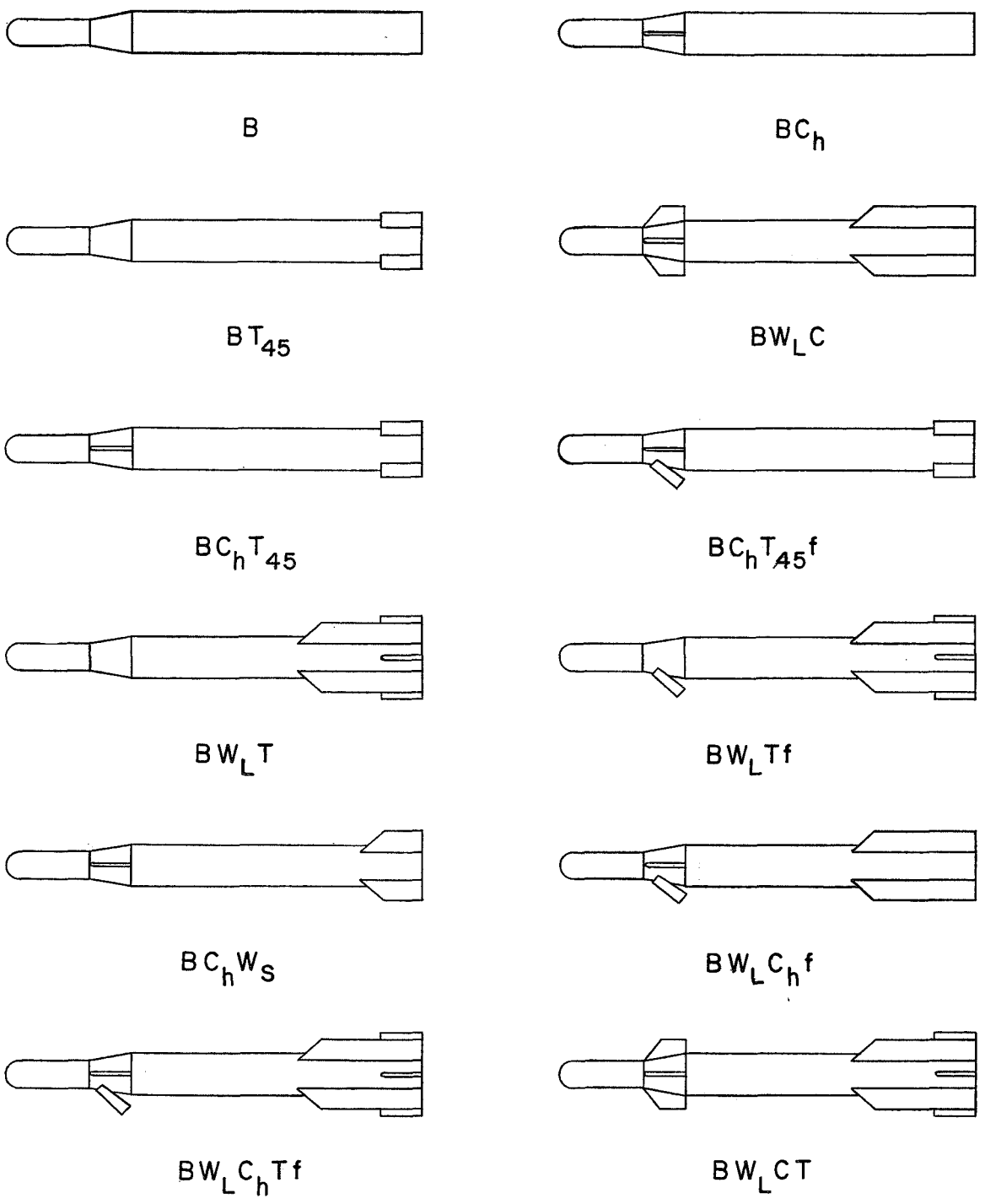

L-1386

Figure 2.- Sketch of configurations investigated.

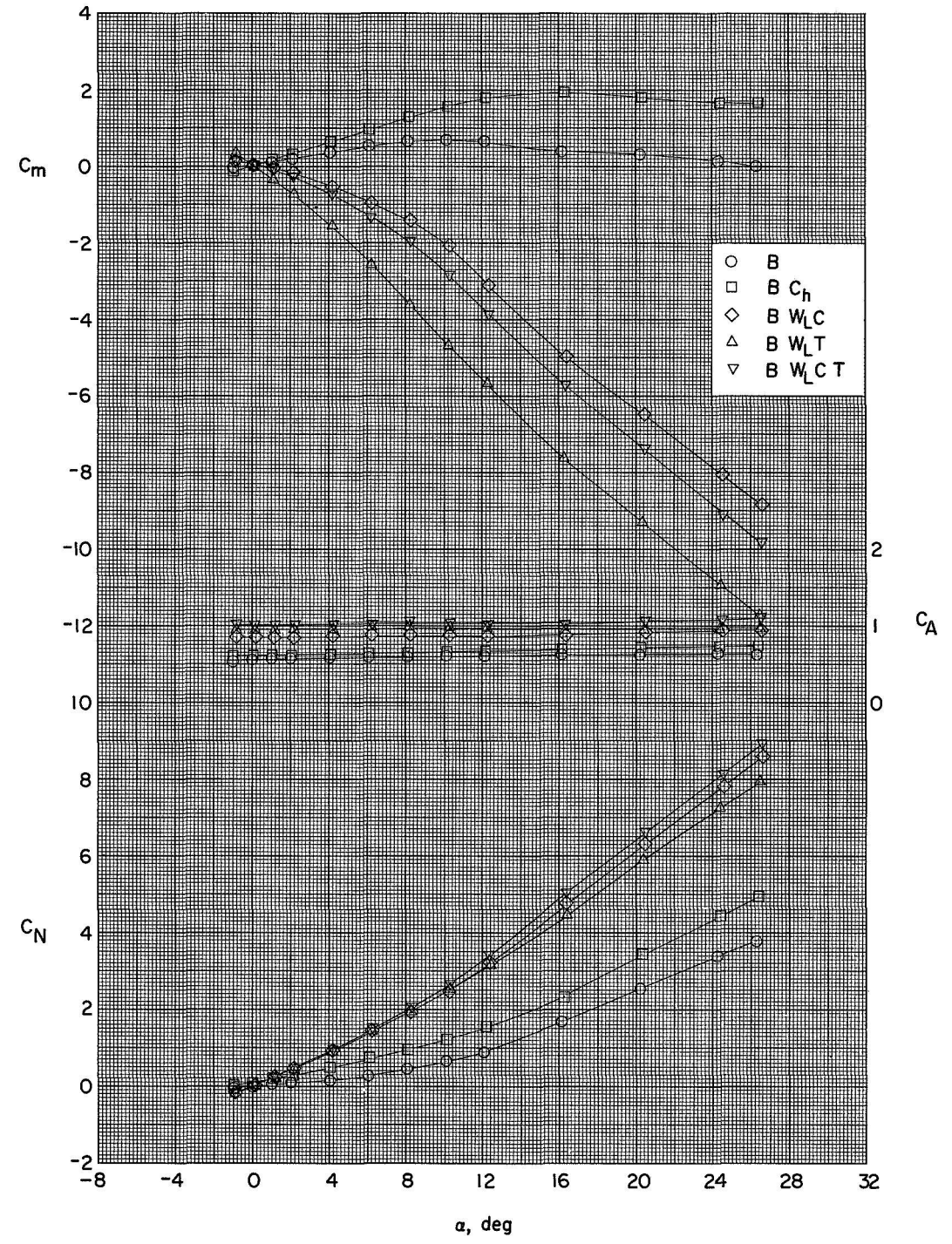

L-1386

Figure 3.- Aerodynamic characteristics in pitch of various combinations of components. All controls at 0° deflection. Large wings.

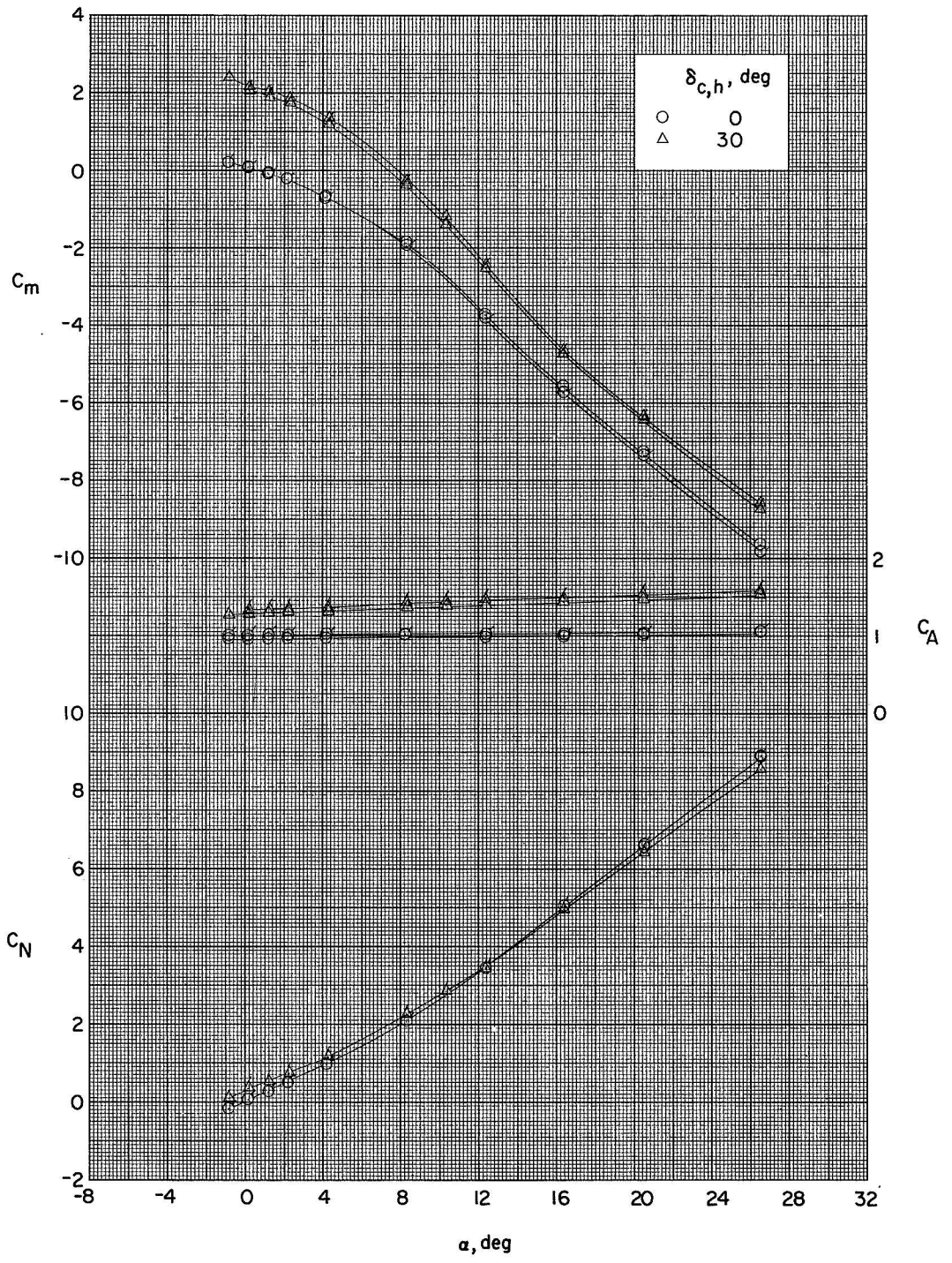

Figure 4.- Effect of ICBM nose shape on the aerodynamic characteristics in pitch of the complete model with large wings. $\delta_{c,v} = \delta_f = \delta_t = 0^o$; BW_LC. Flagged symbols are for spherical nose.

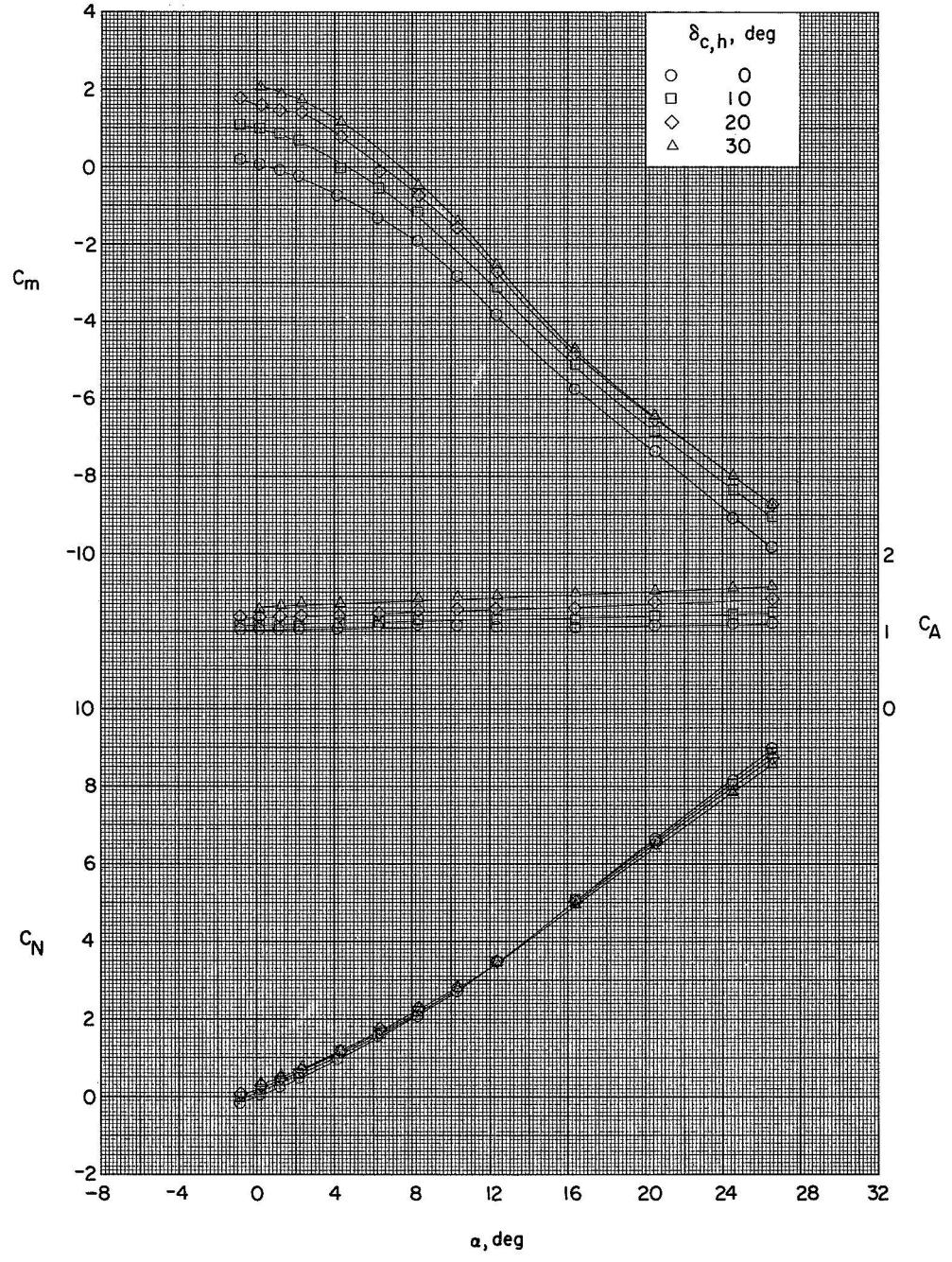

(a) $\delta_{t,h} = 0^{\circ}$.

Figure 5.- Effect of horizontal canard deflection on the aerodynamic characteristics in pitch. Complete model. Large wings; $\delta_f = \delta_{c,v} = 0^{\circ}$; BW_LCT.

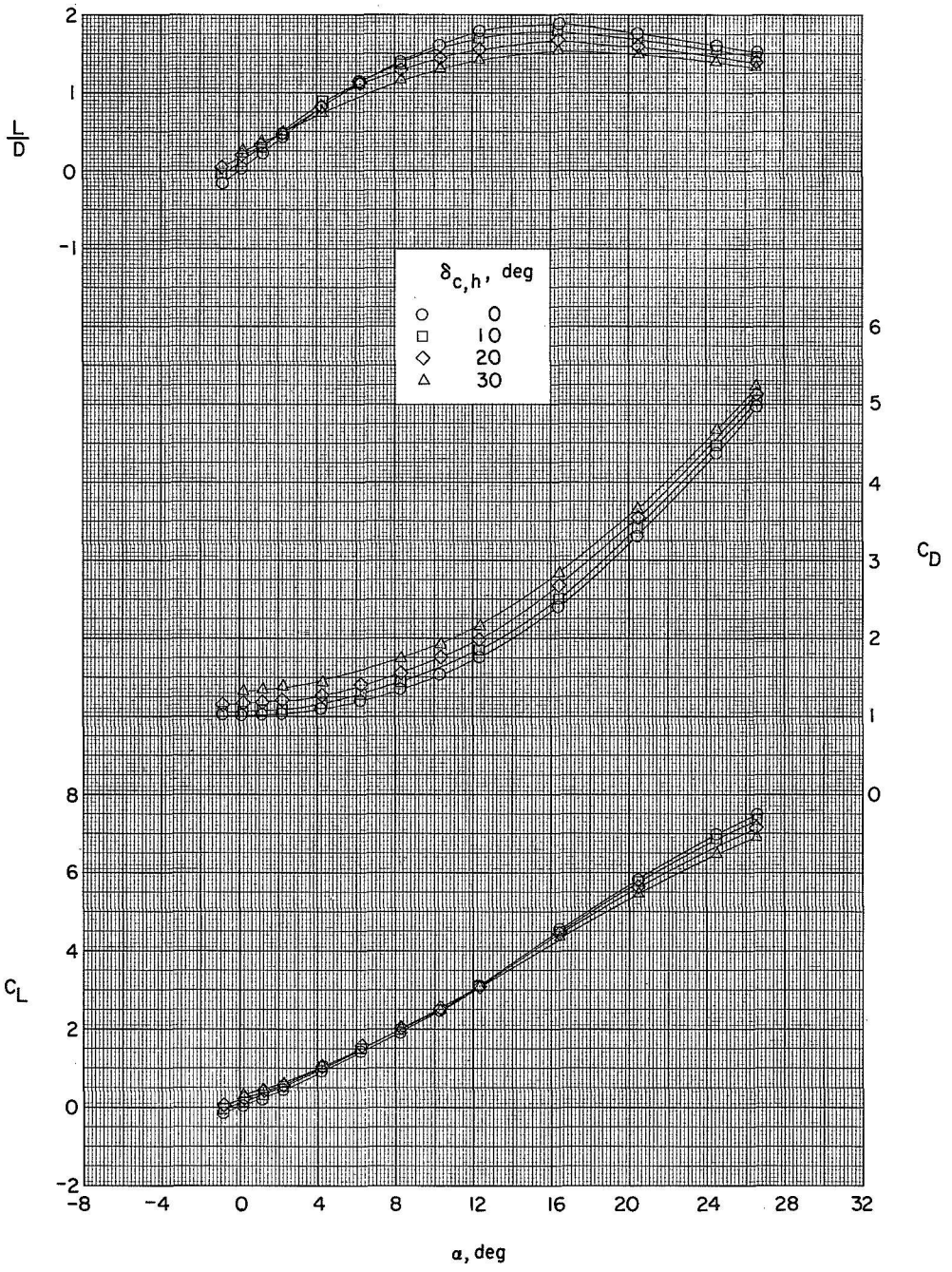

(a) Concluded.

Figure 5.- Continued.

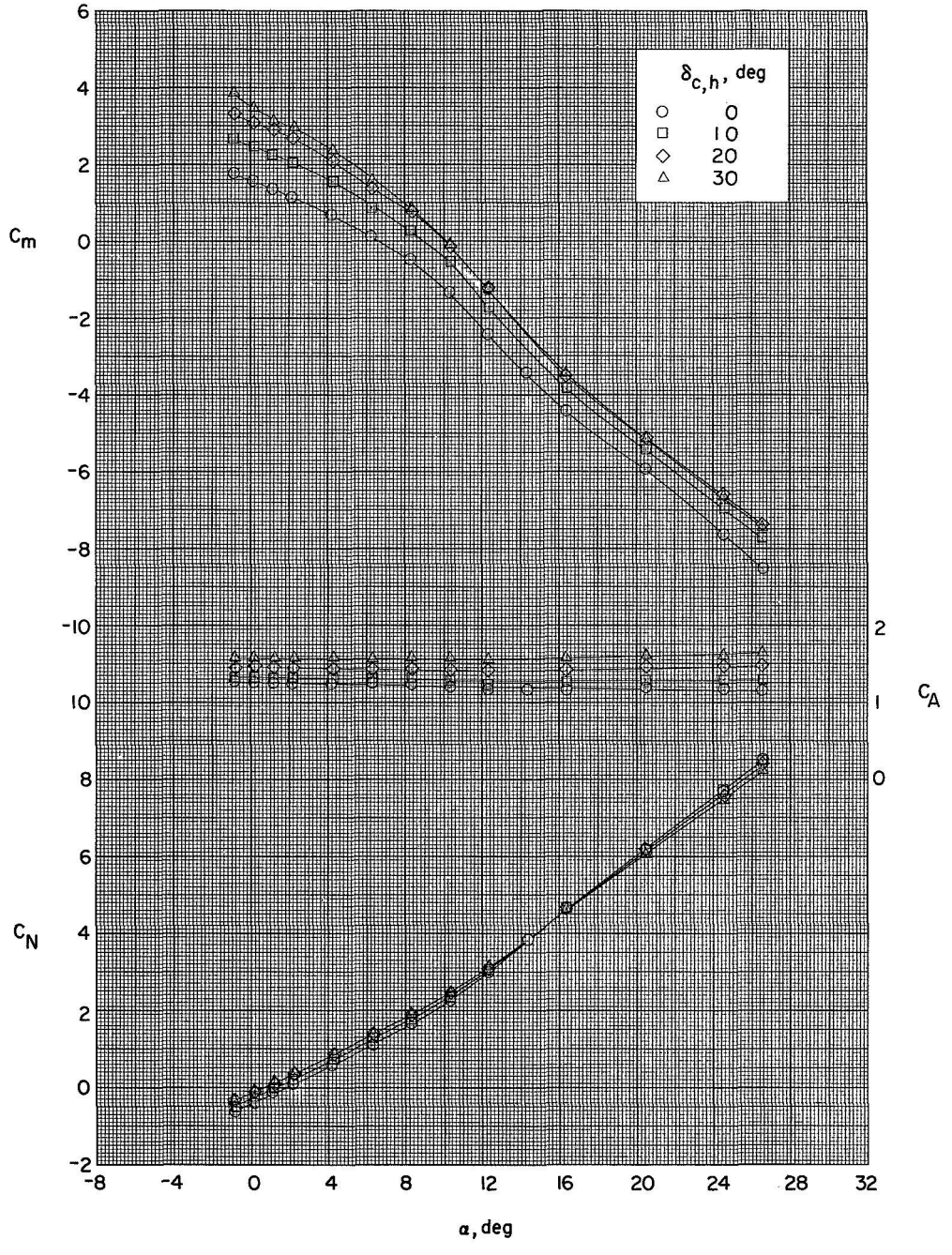

(b) $\delta_{t,h} = -20^{\circ}$.

Figure 5.- Continued.

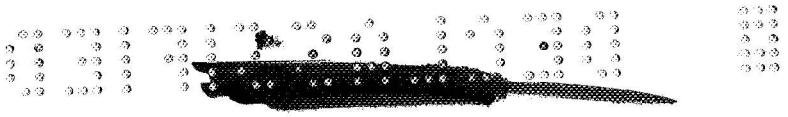

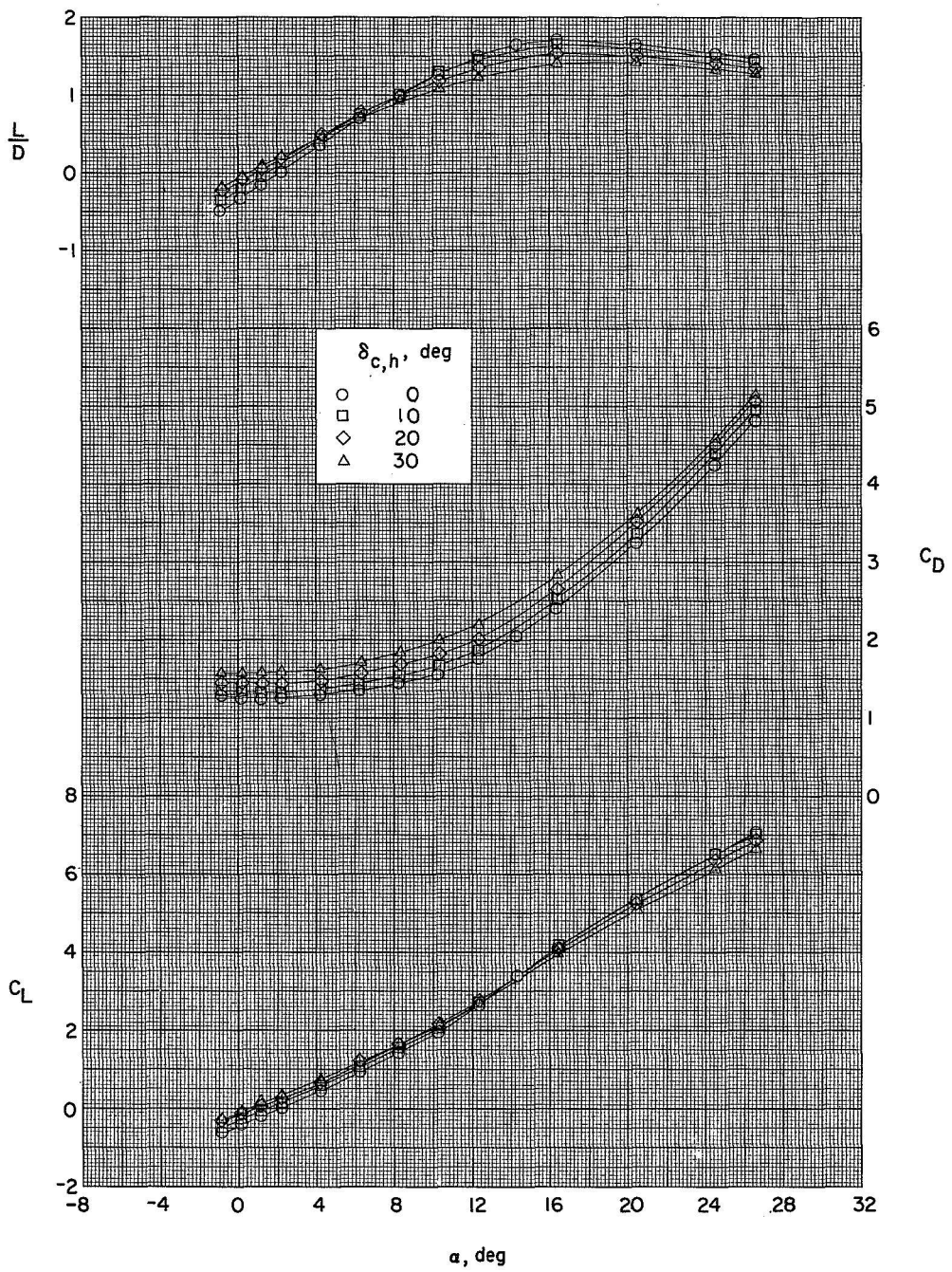

(b) Concluded.

Figure 5.- Concluded.

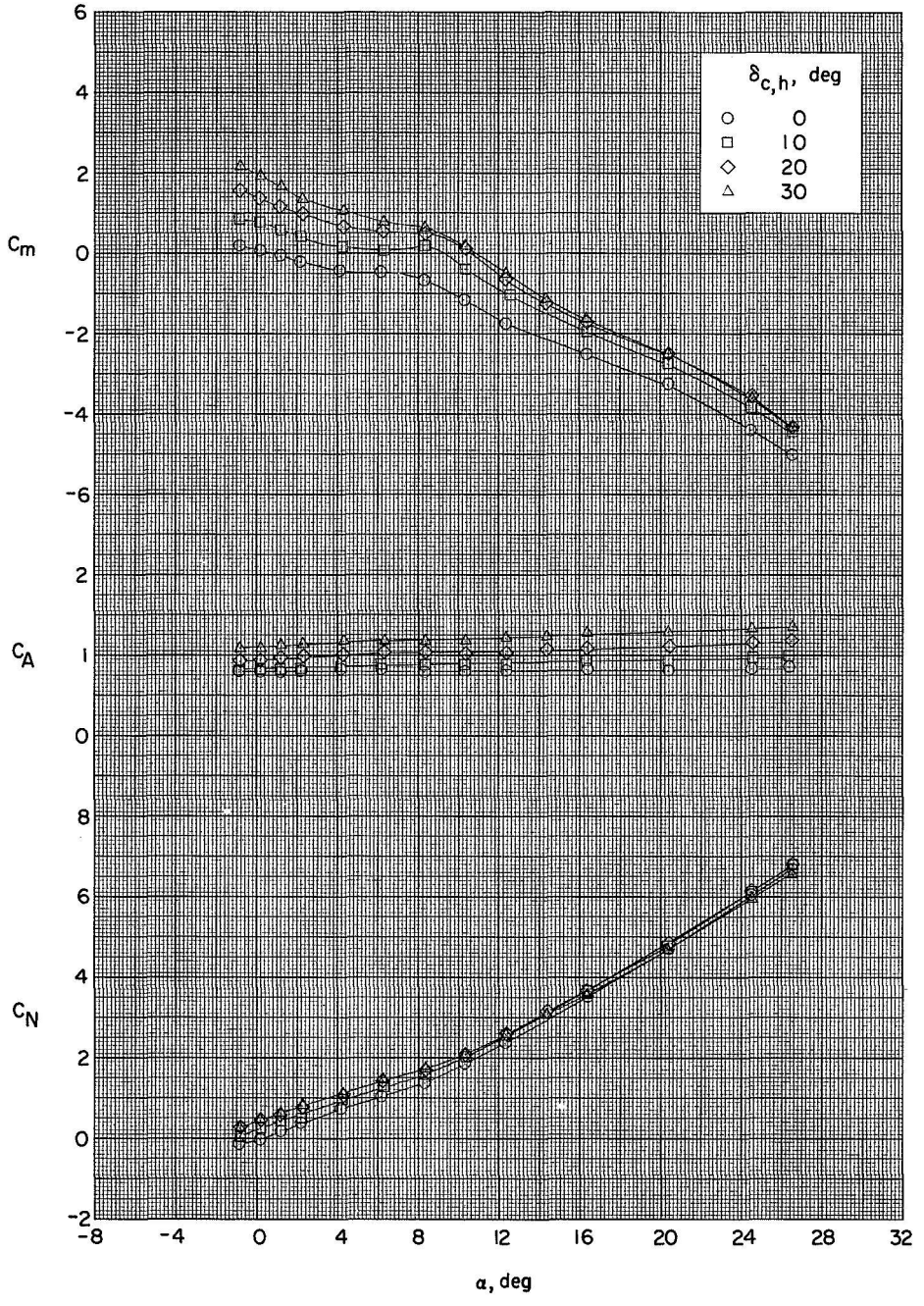

(a) Variation of C_m, C_A, and C_N with α.

Figure 6.- Effect of horizontal canard deflection on the aerodynamic characteristics in pitch. Body—small-wing—horizontal-canard configuration, BC_hW_S.

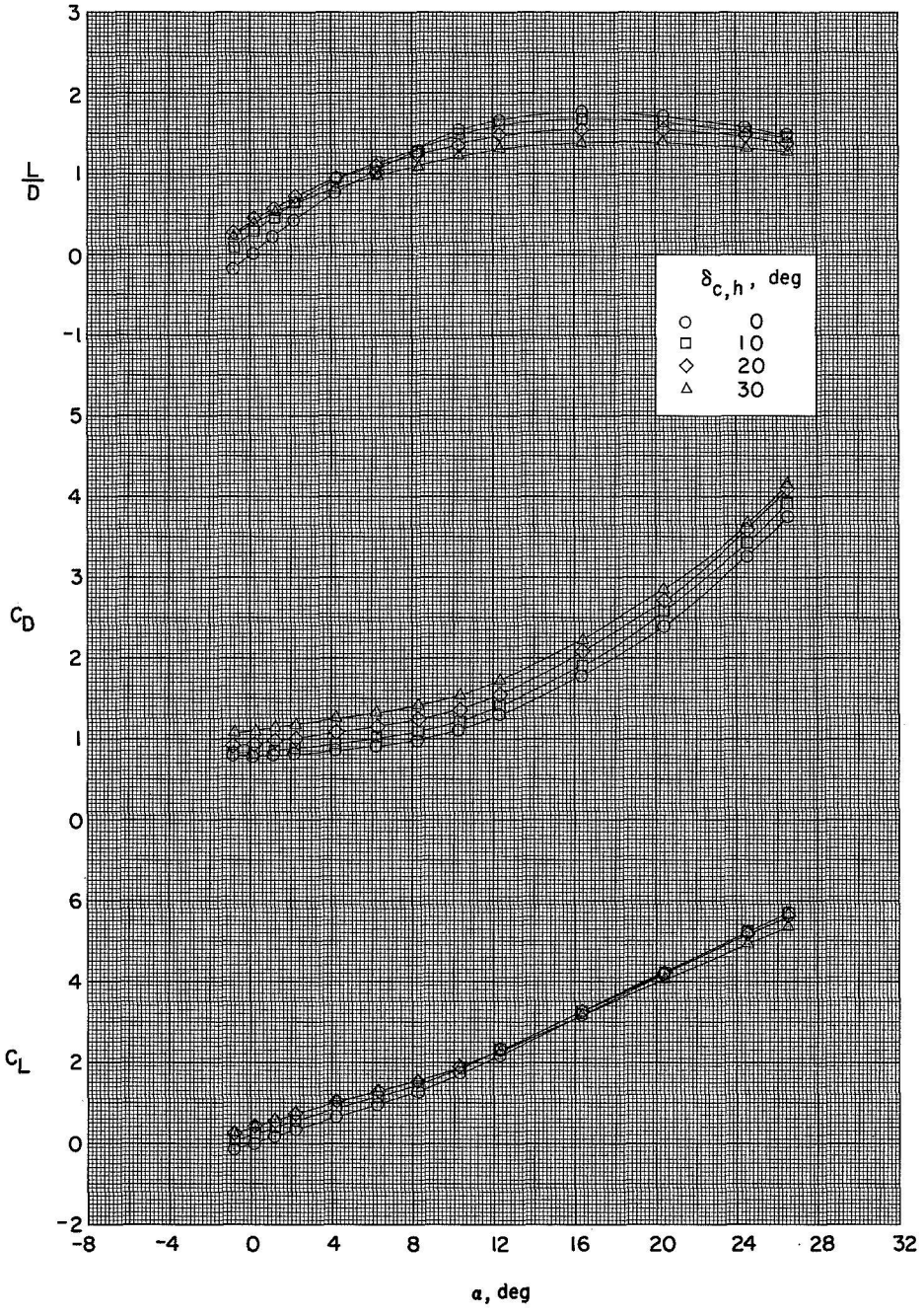

(b) Variation of L/D, C_D, and C_L with α.

Figure 6.- Concluded.

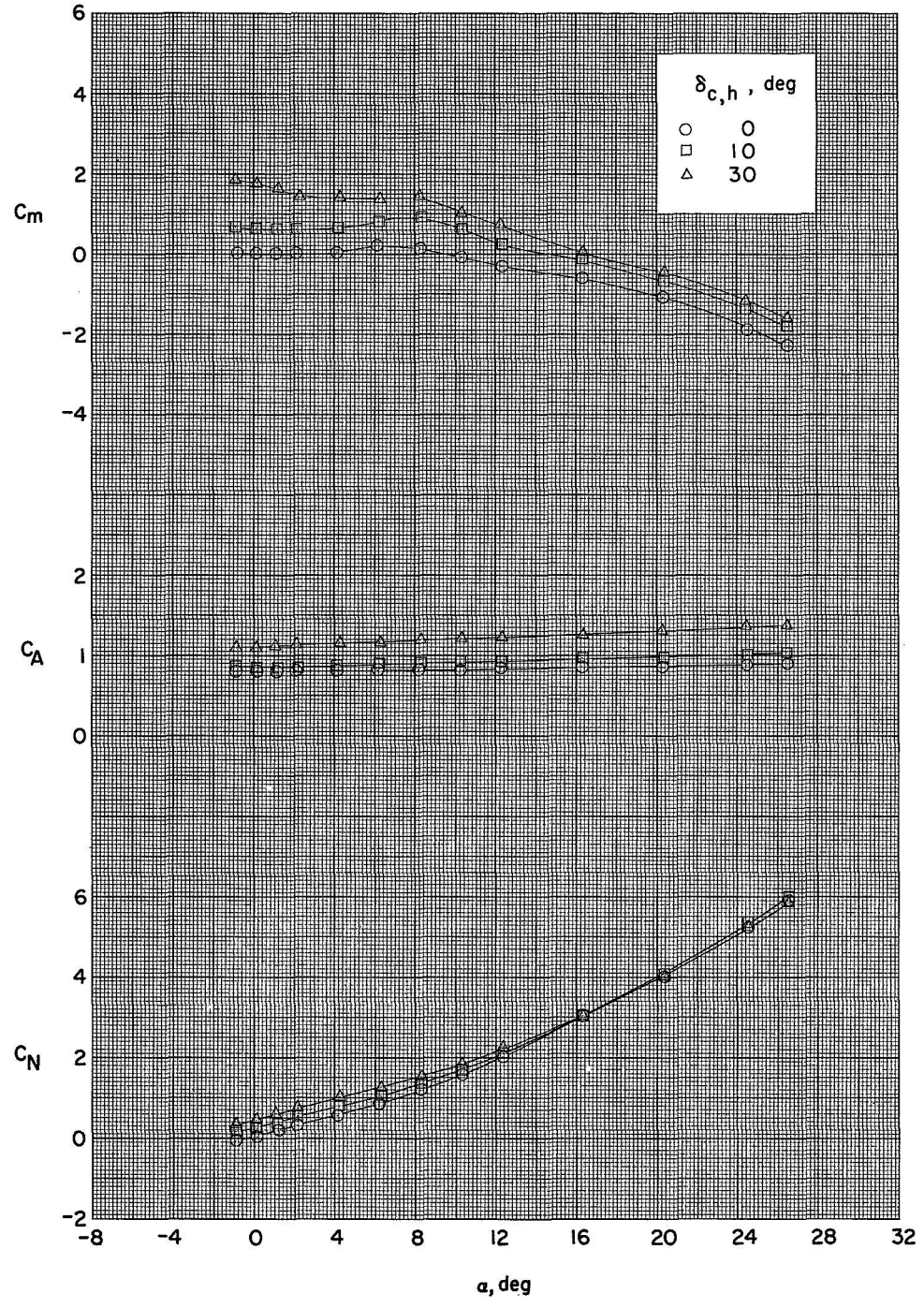

Figure 7.- Effect of horizontal canard deflection on the aerodynamic characteristics in pitch. Body—horizontal-canard—tail configuration; $\delta_t = 0^o$; BC_hT_{45}.

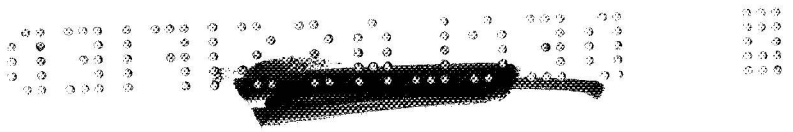

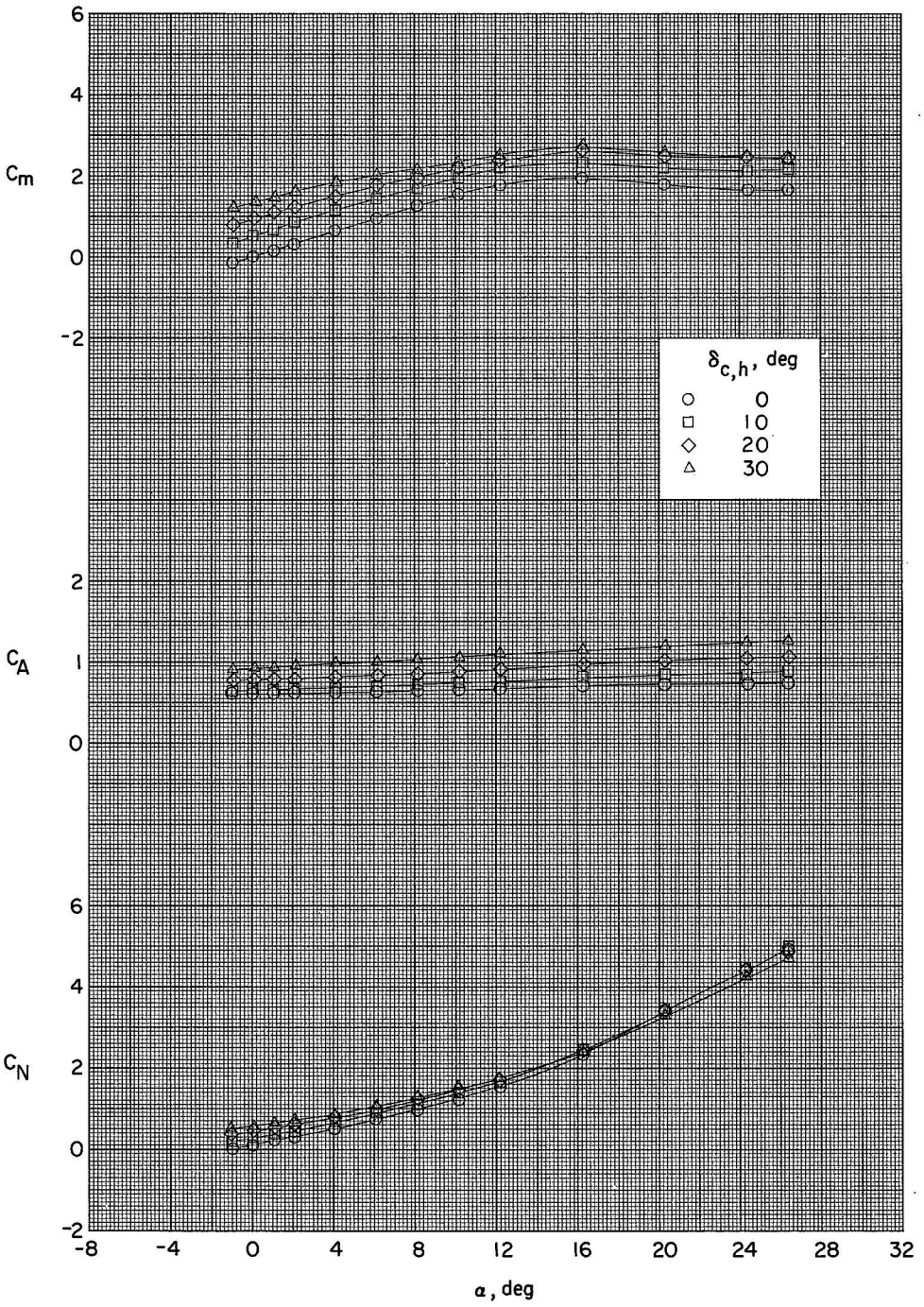

L-1506

Figure 8.- Effect of horizontal canard deflection on the aerodynamic characteristics in pitch. Body—horizontal-canard configuration, BC_h.

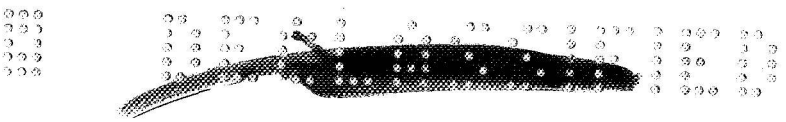

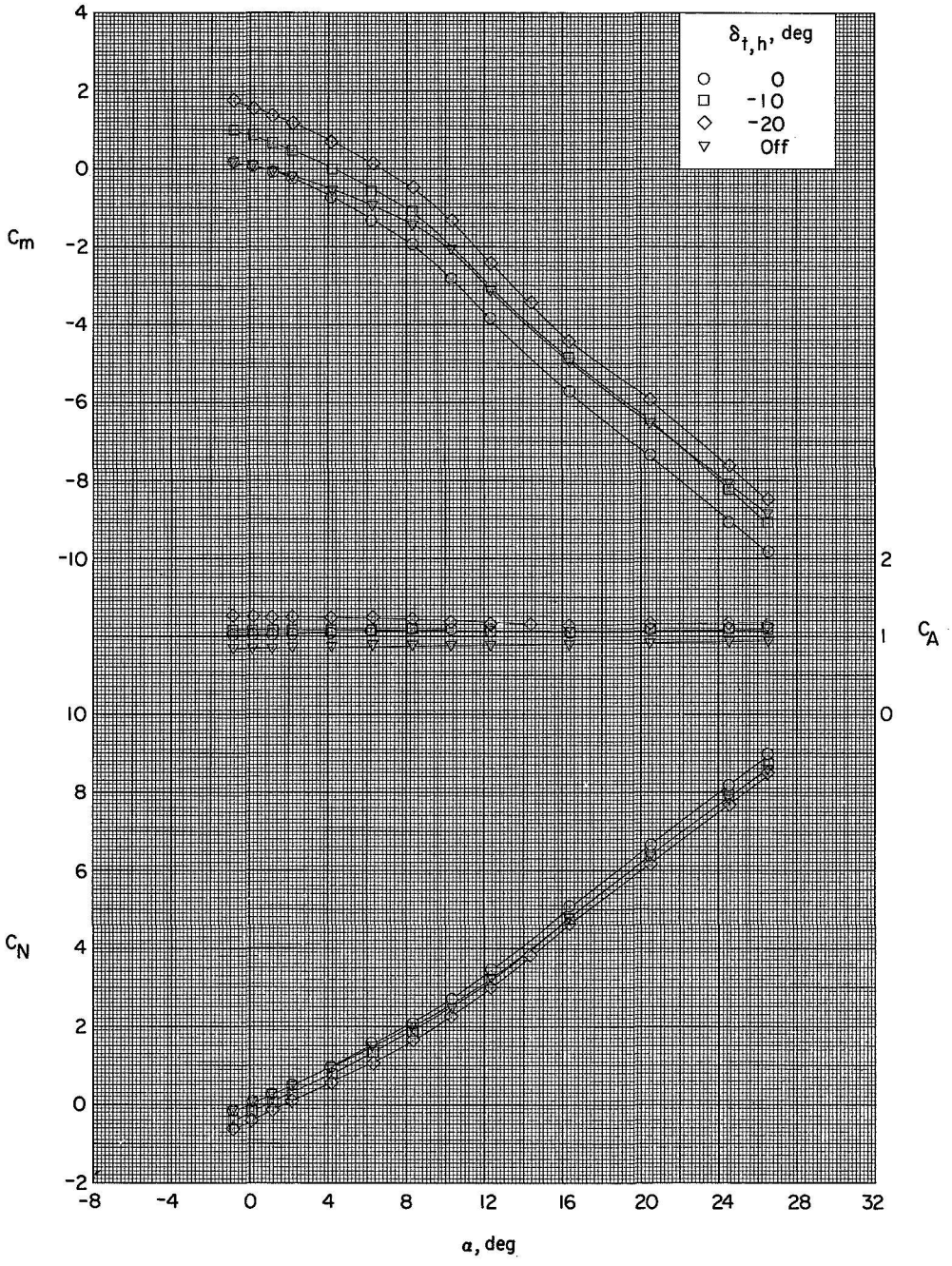

(a) Variation of C_m, C_A, and C_N with α.

Figure 9.- Effect of horizontal-tail deflection on the aerodynamic characteristics in pitch of the complete configuration. Large wings; $\delta_{c,h} = \delta_f = \delta_{t,v} = 0^\circ$; BW_LCT.

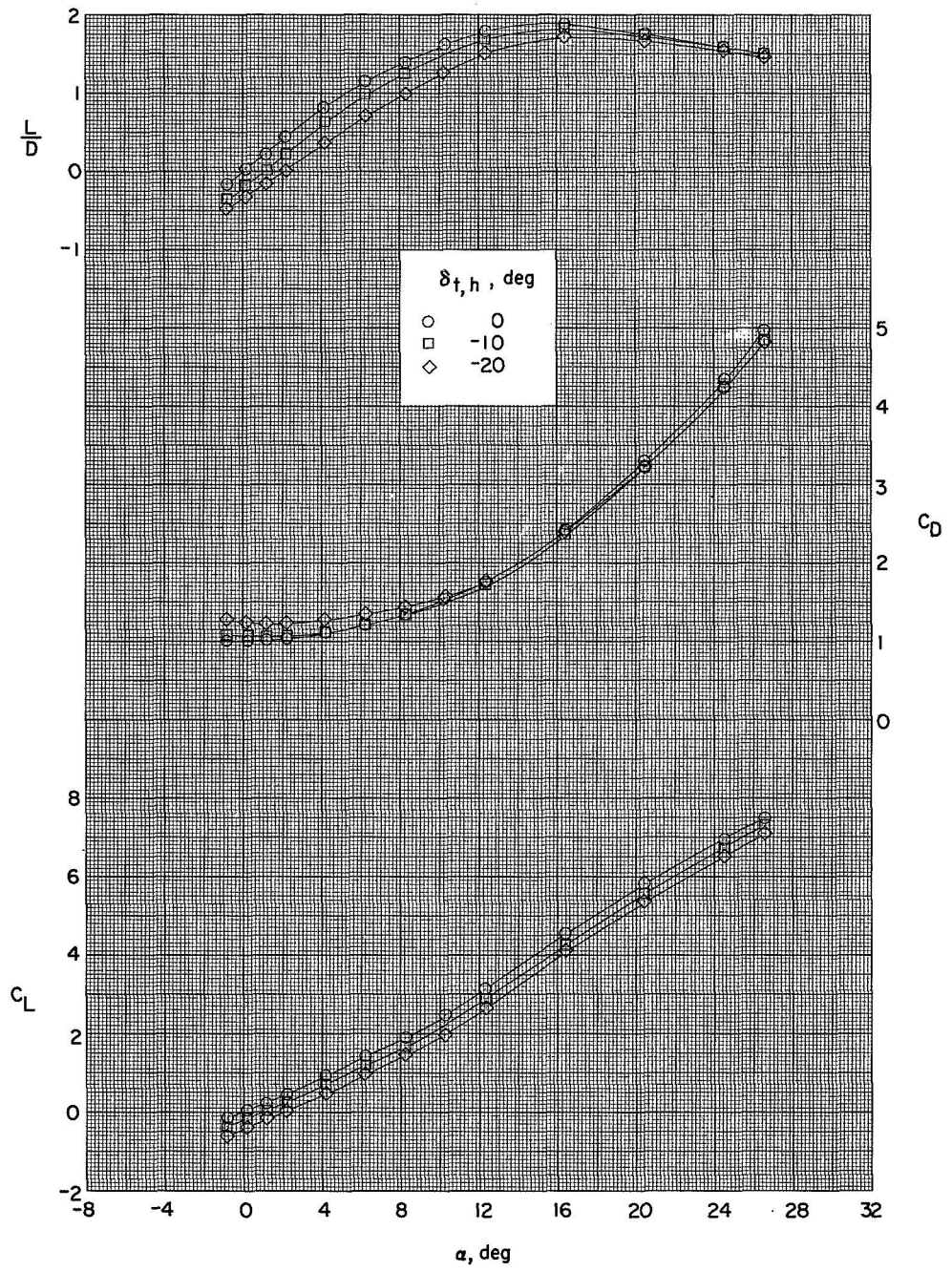

(b) Variation of L/D, C_D, and C_L with α.

Figure 9.- Concluded.

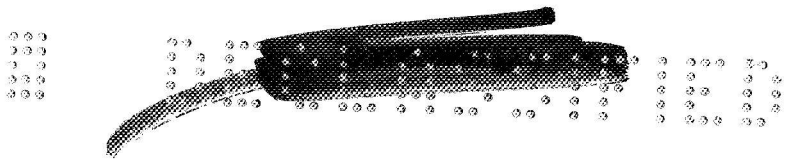

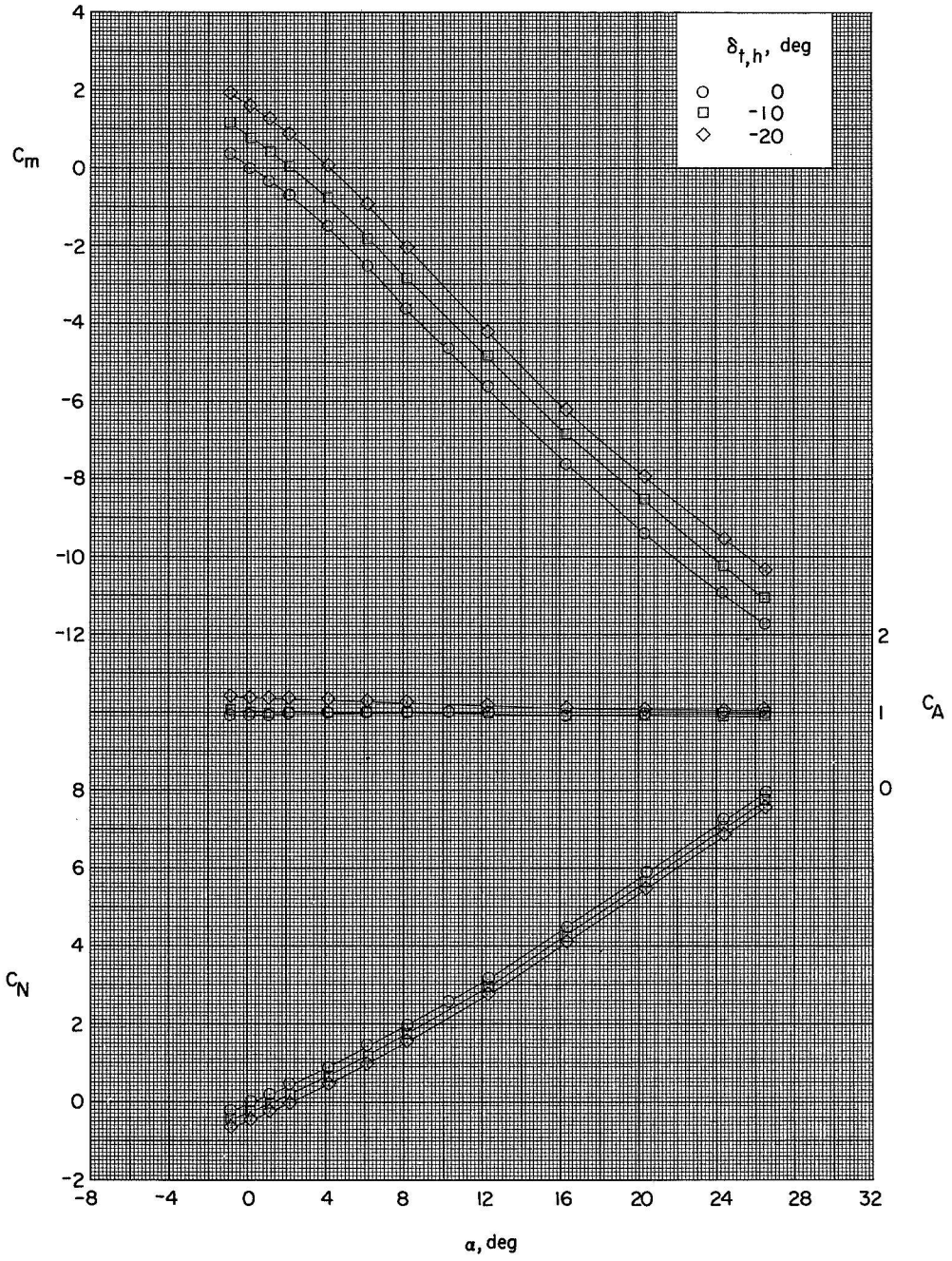

Figure 10.- Effect of horizontal-tail deflection on the aerodynamic characteristics in pitch. Body-wing-tail configuration; large wings; $\delta_f = \delta_{t,v} = 0^o$; BW_LT.

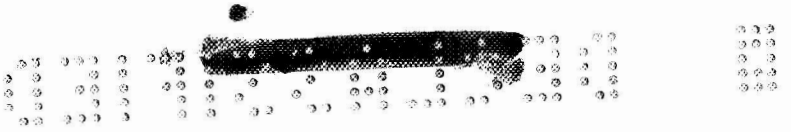

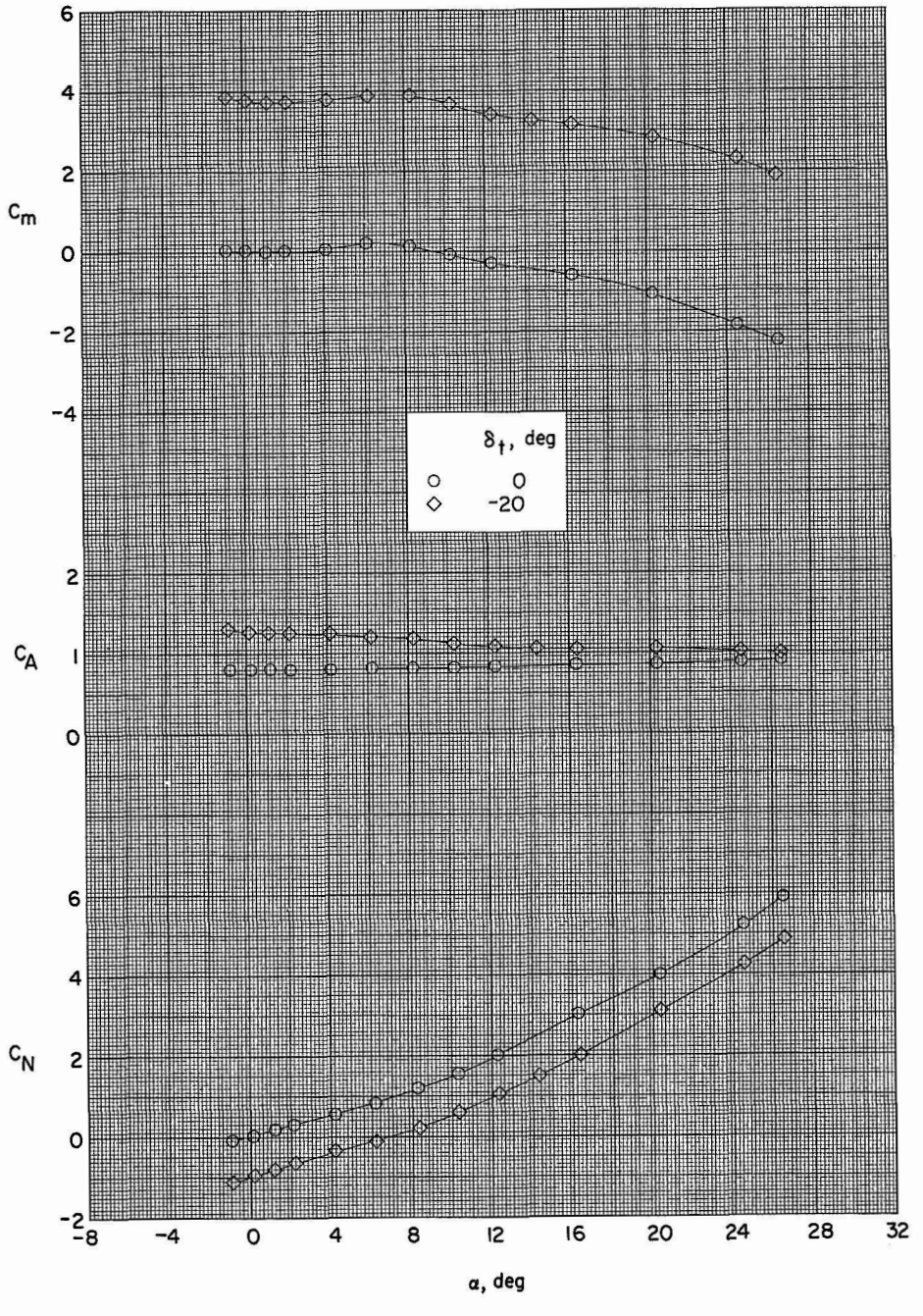

Figure 11.- Effect of tail deflection on the aerodynamic characteristics in pitch. Body—horizontal-canard—tail configuration; tails indexed 45° to body center line; BC_hT_{45}.

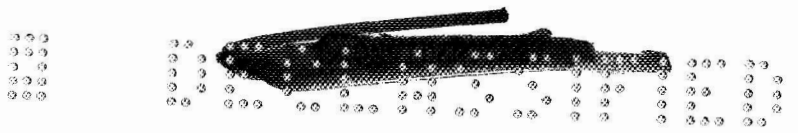

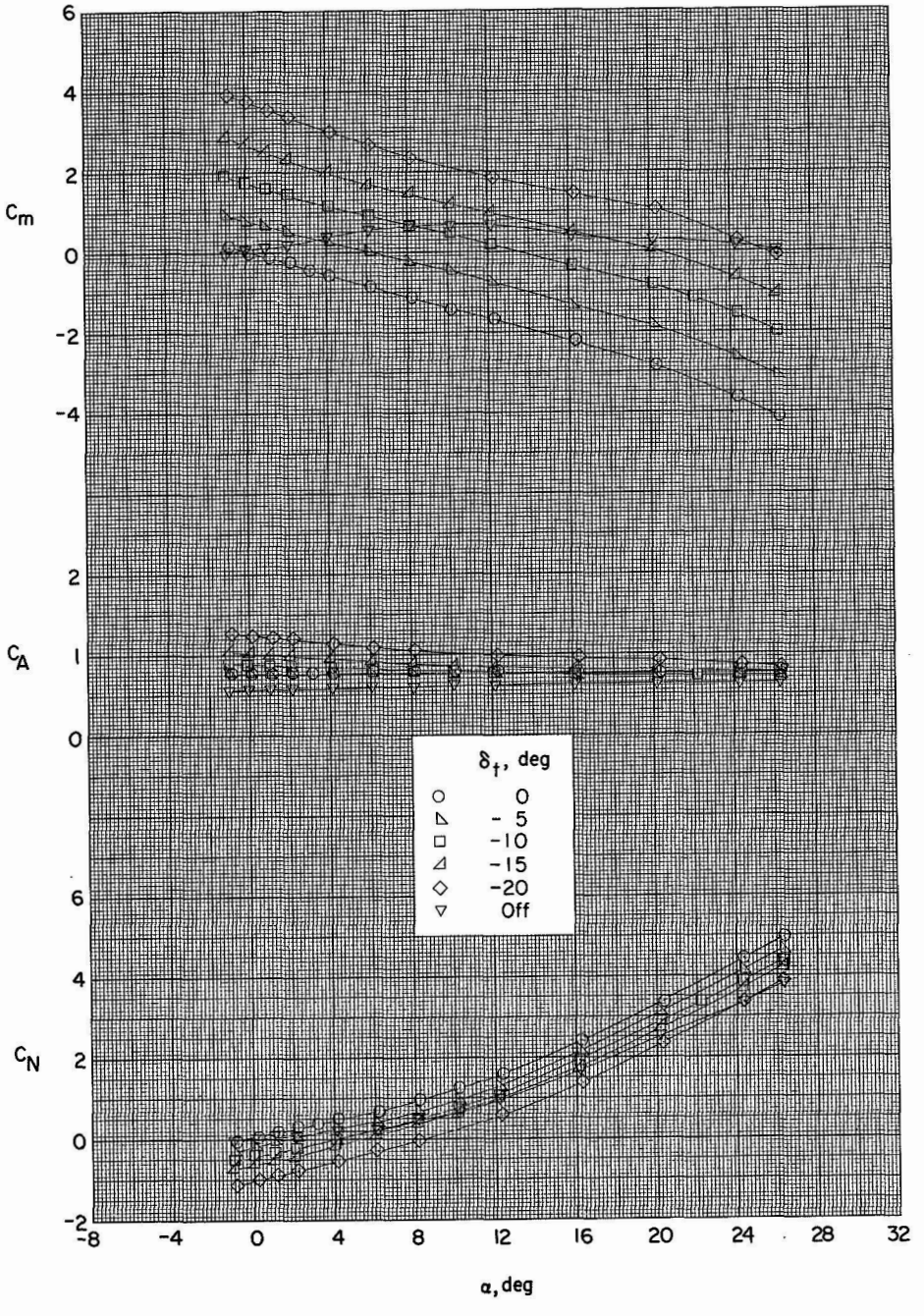

Figure 12.- Effect of tail deflection on the aerodynamic characteristics in pitch. Body-tail configuration; tails indexed 45° to body center line; all tails deflected; BT_{45}.

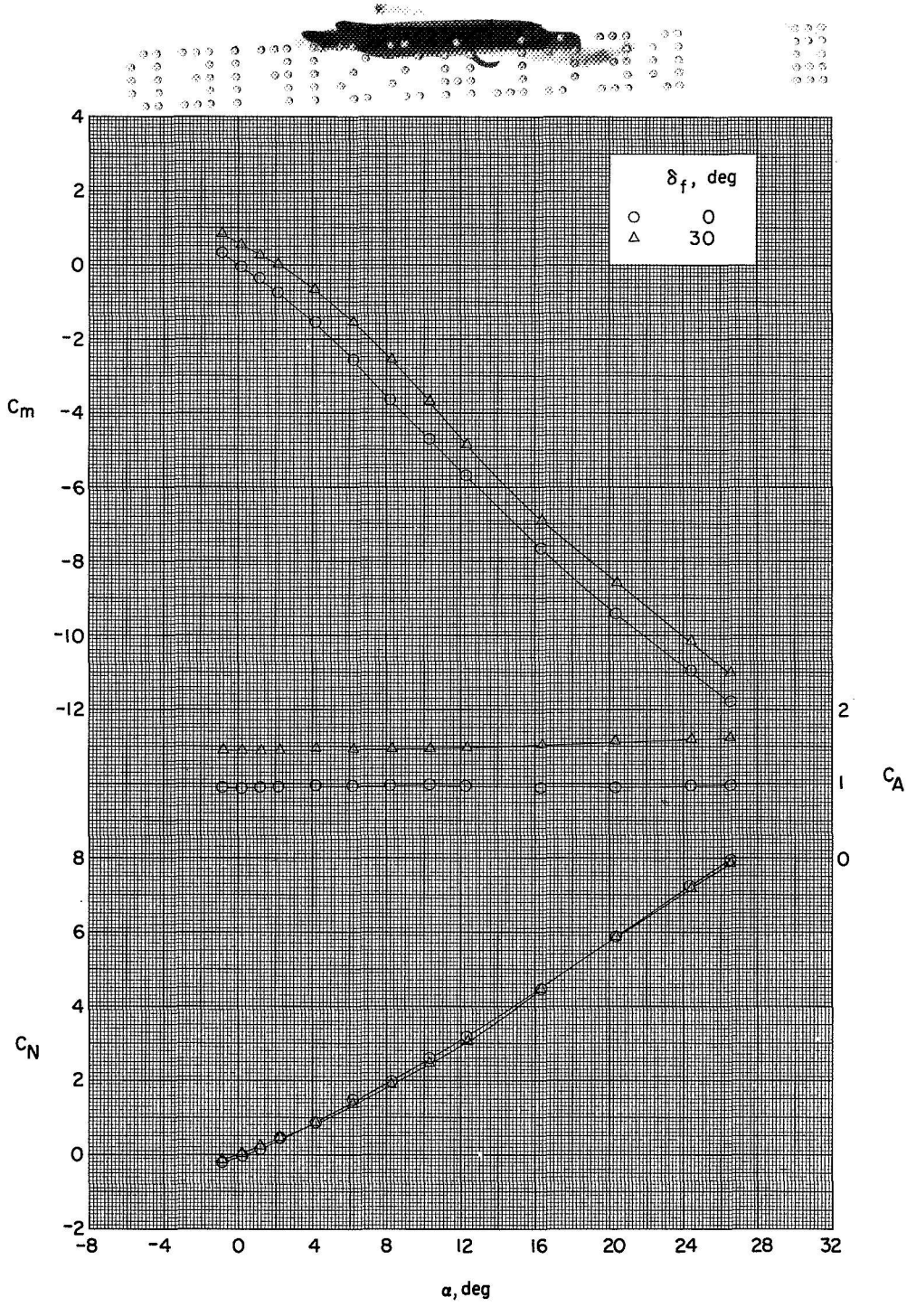

(a) $\delta_{t,h} = 0^{\circ}$.

Figure 13.- Effect of body-flap deflection on the aerodynamic characteristics in pitch. Body-wing-tail configuration; large wings; $\delta_{t,v} = 0^{\circ}$; BW_LTf.

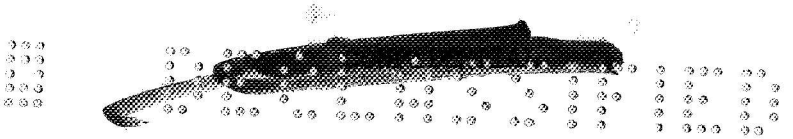

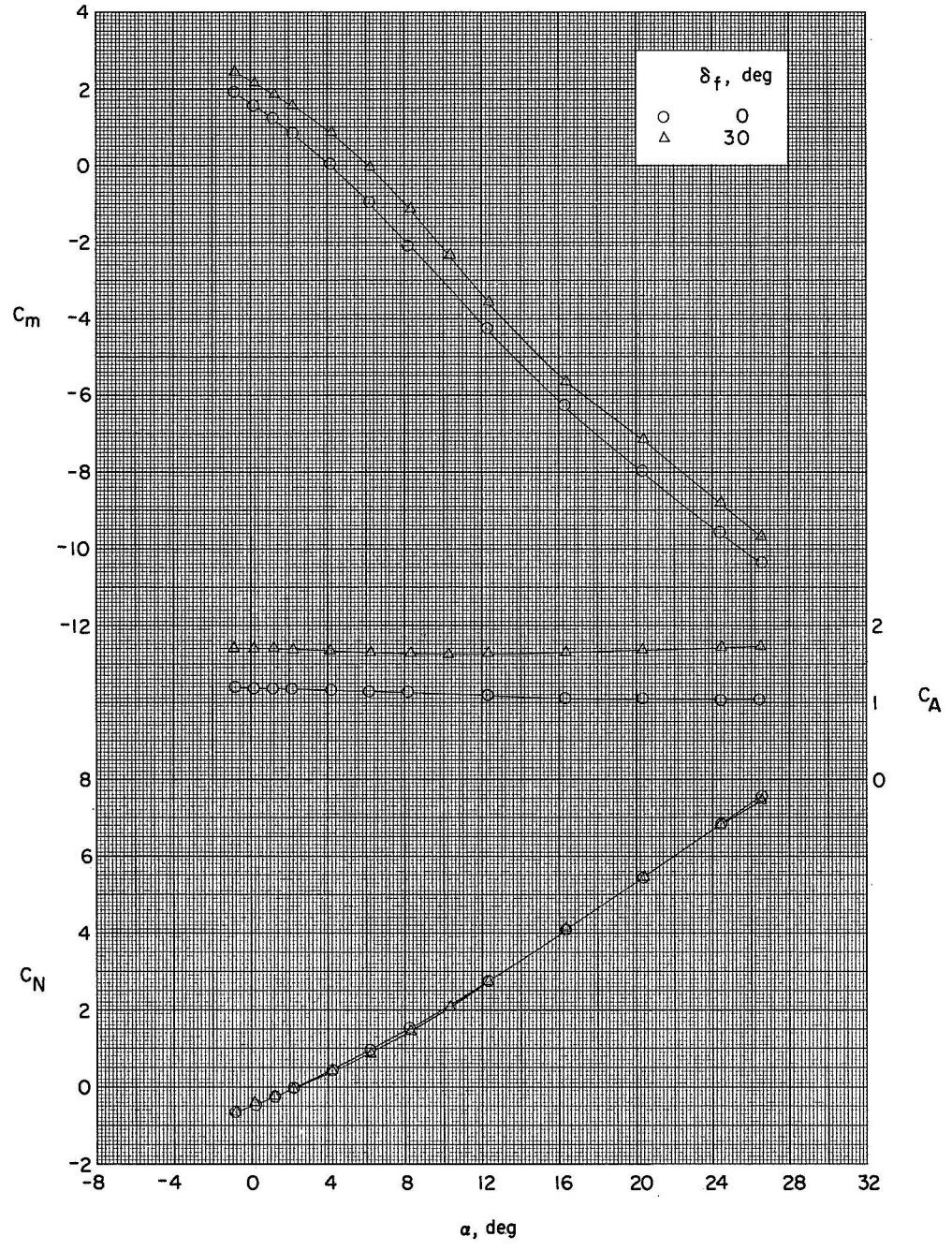

(b) $\delta_{t,h} = -20^{\circ}$.

Figure 13.- Concluded.

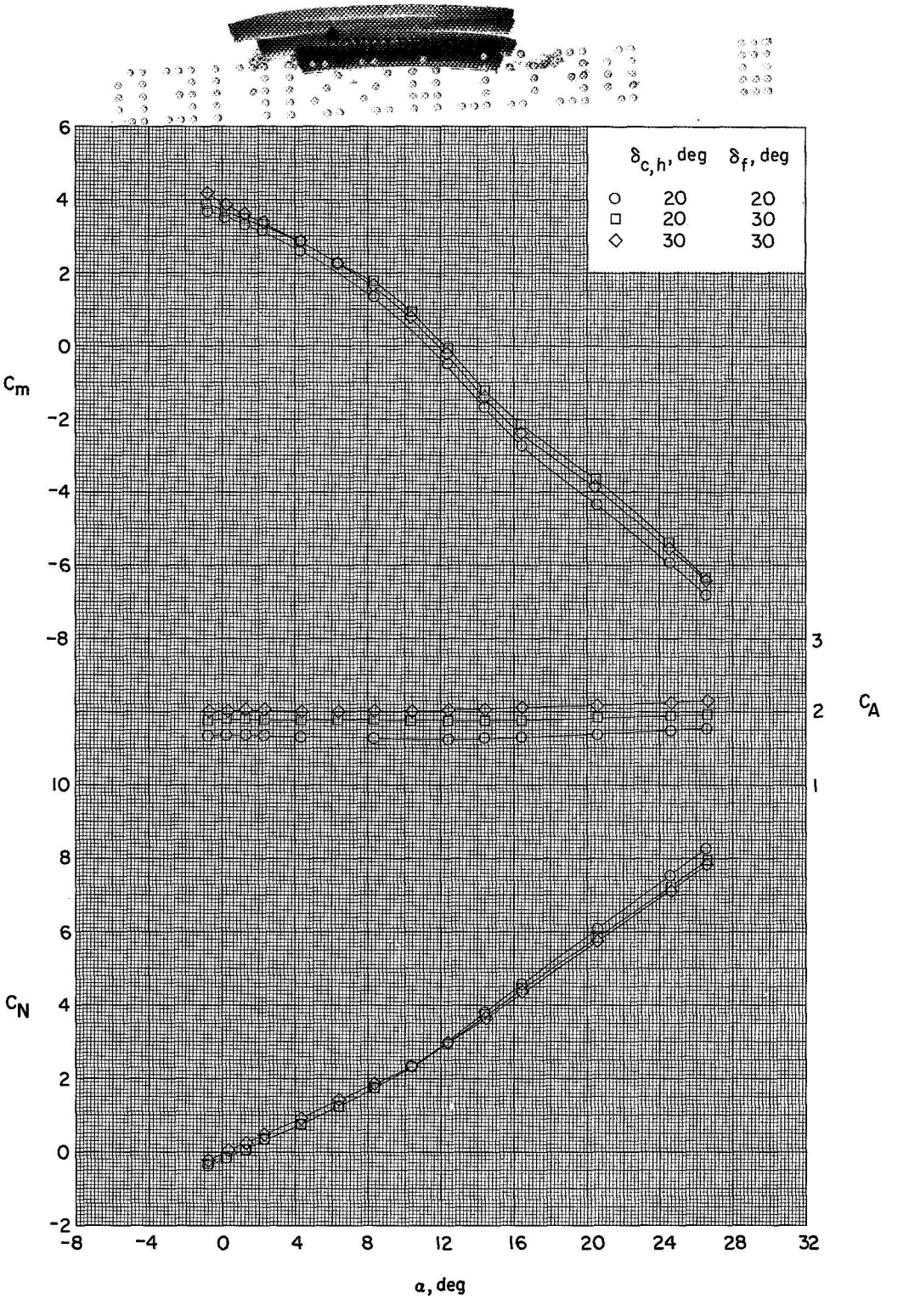

Figure 14.- Effect of combined horizontal-canard and body-flap deflection on the aerodynamic characteristics in pitch. Vertical-canard-off configuration, large wings; $\delta_{t,h} = -20^{o}$; $\delta_{t,v} = 0^{o}$; BW_LC_hTf.

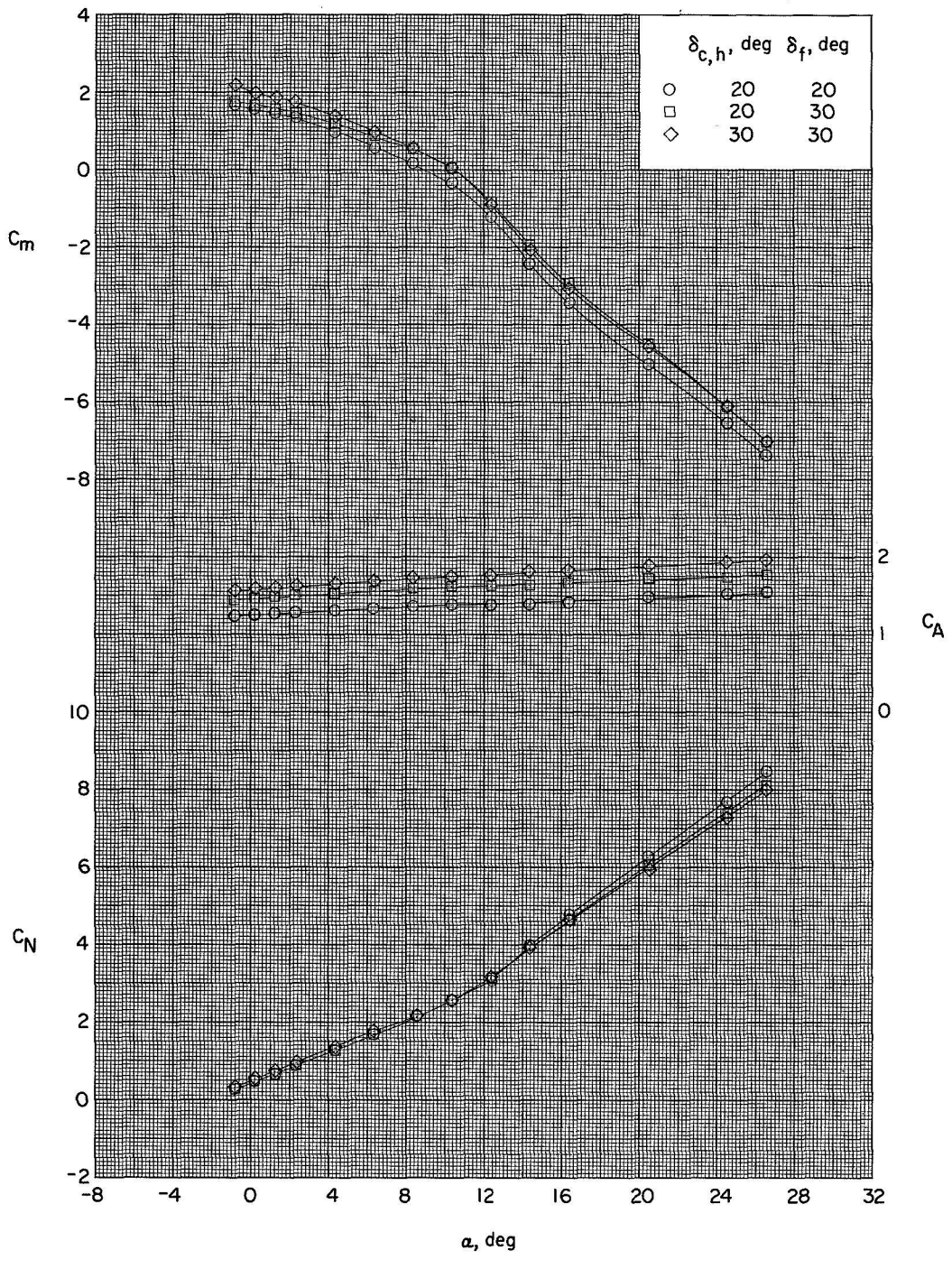

Figure 15.- Effect of combined horizontal-canard and body-flap deflection on the aerodynamic characteristics in pitch. Body—horizontal-canard—wing configuration; large wings; BW_LC_hf.

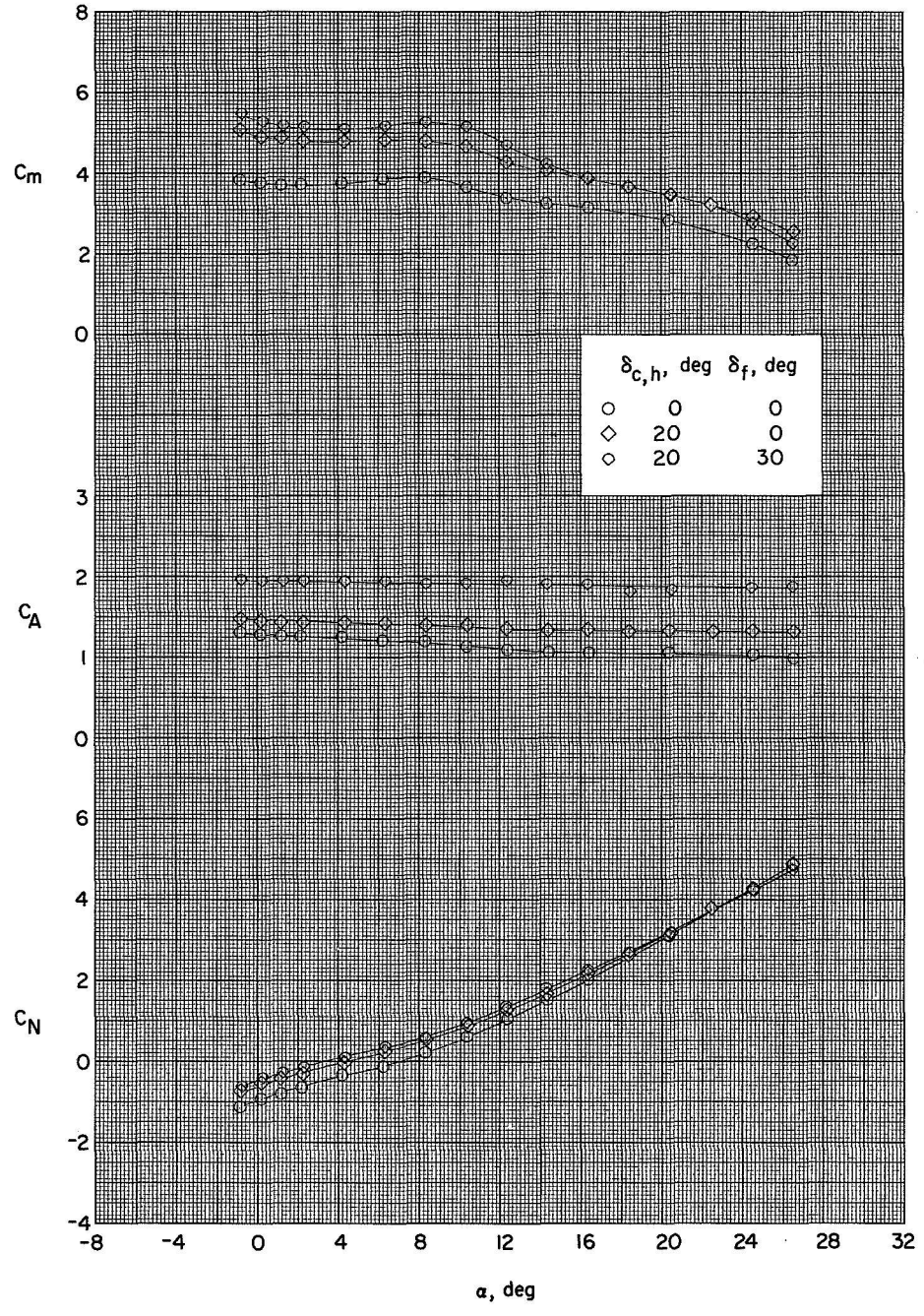

Figure 16.- Effect of combined horizontal-canard and body-flap deflection on the aerodynamic characteristics in pitch. Body—horizontal-canard—tail configuration; $\delta_t = -20^\circ$; tails indexed 45° to body center lines; $BC_hT_{45}f$.

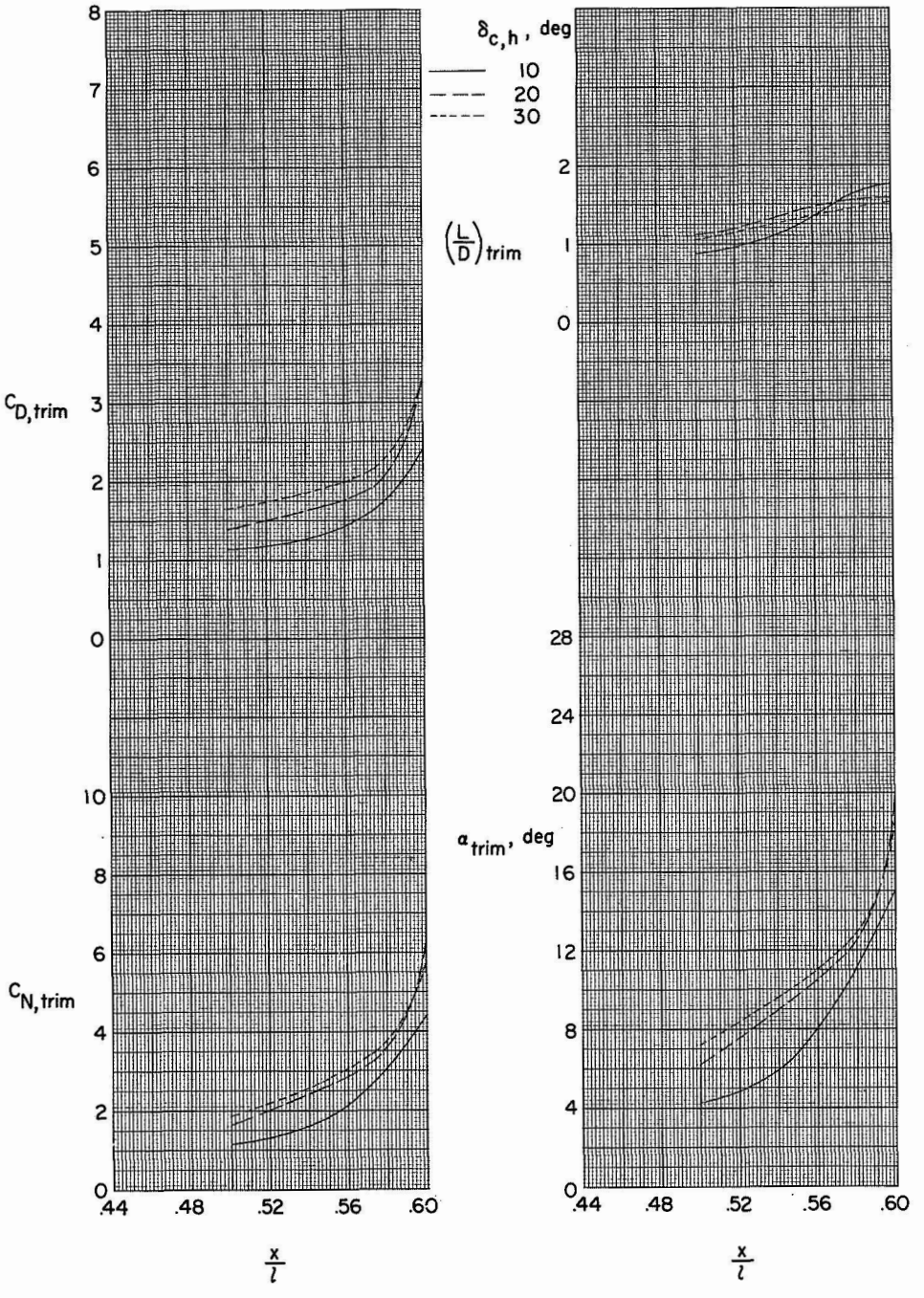

(a) BW_LCT; $\delta_{t,h} = 0^\circ$.

Figure 17.- Variation of longitudinal trim characteristics with moment reference point location for various configurations.

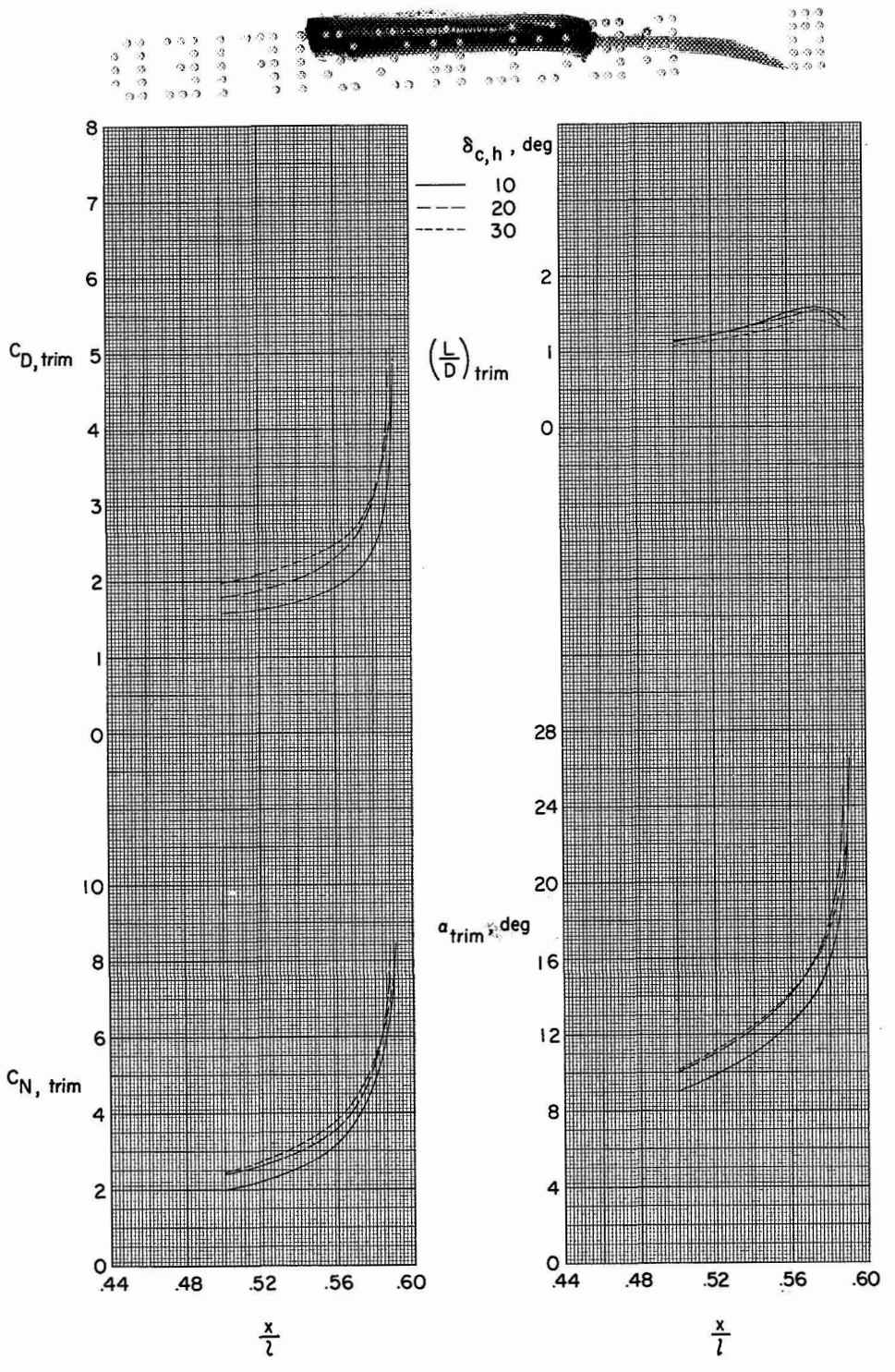

(b) BW_LCT; $\delta_{t,h} = -20^o$.

Figure 17.- Continued.

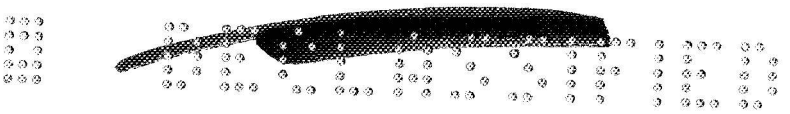

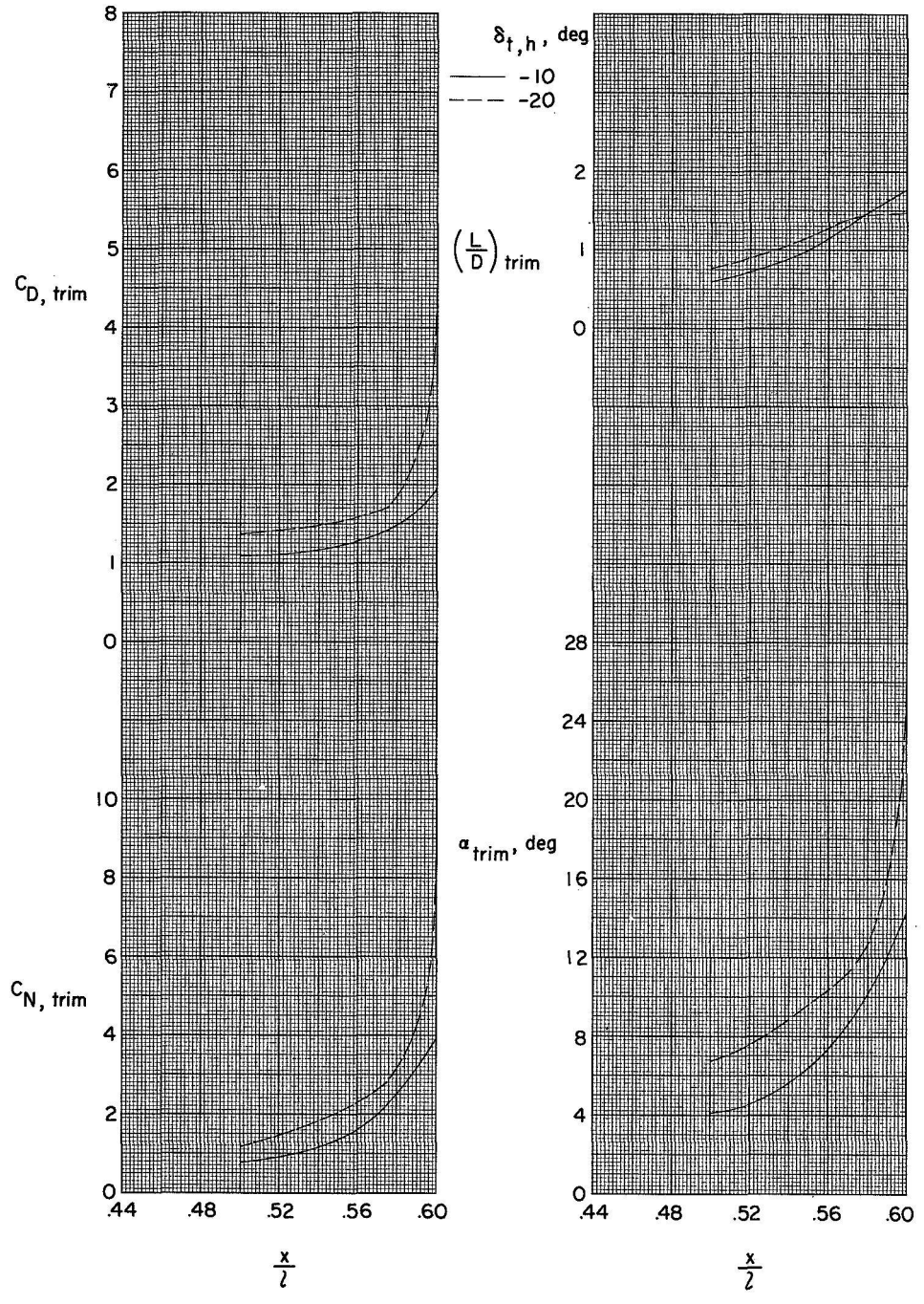

(c) BW_LCT; $\delta_{c,h} = 0^\circ$.

Figure 17.- Concluded.

NASA - Langley Field, Va. L-1386